



universität  
wien

# DISSERTATION

Titel der Dissertation

„In situ ATR-FTIR spectroscopy study of organic and biological molecule-layers used in nanoscale biosensors and determination of surface concentrations“

Verfasser

Mag. Manuel Punzet

angestrebter akademischer Grad

Doktor der Naturwissenschaften (Dr.rer.nat.)

Wien, 2014

Studienkennzahl lt. Studienblatt: A 091 490

Dissertationsgebiet lt. Studienblatt: Molekulare Biologie

Betreuerin / Betreuer: Prof. Dr. Annette Rompel

## **Danksagung**

Ich möchte mich zu aller erst herzlich bei meinem Betreuer Dr. Dieter Baurecht bedanken, welcher mich immer bedingungslos unterstützt hat und immer ein offenes Ohr für Fragen hatte. Weiters bei Prof. Annette Rempel, für ihre scheinbar endlose Geduld. Meinen ehemaligen Kollegen Dr. Ladislav Habala, Dipl.Chem. Christian Molitor, Mag. Stefan Mauracher und Dr. Alfred Hummer danke ich sehr herzlich für ihre Unterstützung und das angenehme zwischenmenschliche Klima am Institut für Biophysikalische Chemie. Besonders danken möchte ich Ing. Regina Prossinagg für ihre moralische und menschliche Unterstützung während meiner Dissertationszeit. Dr. Clemens Heitzinger möchte ich für seine hervorragende Projektleitung im FWF Projekt P20871-N31 danken.

## Table of content

Abstract .....	5
1 Introduction .....	8
1.1 Biosensors .....	8
1.2 Aim of this work and questions .....	10
1.3 Experimental strategy .....	11
1.4 FTIR-ATR spectroscopy .....	13
2 Methods and materials .....	15
2.1 Chemicals used in this work .....	15
2.1.1 Bovine serum albumin .....	15
2.1.2 Tumor necrosis factor alpha (TNF- $\alpha$ ) .....	16
2.1.3 Prostate specific antigen (PSA) .....	17
2.2 Multiple internal reflection elements (MIREs) .....	18
2.3 IR interaction with water .....	20
2.4 Calculation of the surface concentration [34] .....	21
2.5 SBSR measurement method .....	23
2.6 Transmission spectrometer setup .....	25
2.7 IR-ATR spectrometer setup .....	26
2.9 Preparation of silicon ATR-elements .....	30
2.10 Schemes of silane modifications .....	31
2.11 Experimental procedure for silanisation of silicon ATR-elements using 3-(trimethoxy) butylsilyl aldehyde .....	32
2.12 Passivation of silane aldehyde surface .....	33
2.13 BSA saturation experiments .....	34
2.14 Experimental procedures for BSA saturation experiments .....	35

2.15 Protein binding to silan aldehyde surface .....	36
2.15.1 Experimental procedures for the biotin/streptavidin system.....	36
2.15.2 Experimental procedures for hTNF- $\alpha$ antibody and antigen system .....	37
2.15.3 Experimental procedures for the PSA-antibody and PSA system.....	39
2.16 Experimental procedures for DNA-recognition system .....	40
3 Results and Discussion .....	44
3.1 Surface concentration of 3-(trimethoxy)butylsilyl aldehyde.....	44
3.2 Surface concentrations of BSA on blank silicon and germanium surfaces .....	47
3.3 Bovine serum albumin (BSA) on aldehyde silane layer .....	49
3.4 Surface concentration of covalently bound BSA on aldehyde silane surface .	52
3.5 Insulin on aldehyde-silane layer.....	53
3.6 Streptavidin-Biotin on aldehyde silane layer .....	56
3.7 Surface concentrations of TNF- $\alpha$ anti-body on silanised silicon and captured TNF- $\alpha$ .....	60
3.8 PSA-antibody and PSA on aldehyde surface .....	65
3.9 Passivation of antibody surface with ethanolamine .....	67
3.10 DNA binding and corresponding sequence detection .....	68
4 References .....	71
Curriculum vitae .....	75
Publication “Determination of surface concentrations of individual molecule-layers used in nanoscale biosensors by in situ ATR-FTIR spectroscopy (Nanoscale 2012)”	

## Abstract

Biosensors of the nanowire type with gate electrodes in contact to the analyzing species are promising tools to determine molecule concentrations down to the femtomolar range. FTIR-ATR spectroscopy was used to study the surface modification protocols and protein binding possibilities of prototype nanosensors. The single-beam sample-reference method was used to compensate absorptions of water vapor, solvent absorption and inhomogeneities in the used multiple internal reflection element (MIRE). In a step-by-step process silicon and germanium MIREs were modified with a silane linker to covalently bind various protein molecules to the surface to mimic a biosensor setup.

In preliminary experiments the adhesion behavior of bovine serum albumin (BSA) on polished and silane modified silicon surfaces was studied. In further BSA experiments the concentration of additional sodium chloride was varied and the resulting surface concentrations measured. Measured surface concentrations for BSA ranged from  $1.5 \text{ e-}12$  to  $2.4 \text{ e-}12 \text{ Mol/cm}^2$ . In subsequent experiments protein-ligand systems with specific binding behavior such as streptavidin/biotin, tumor necrosis factor  $\alpha$ /antibody and prostate specific antigen (PSA)/antibody were attached to the silan and the surface concentrations determined. To inhibit unspecific adhesion of protein molecules the silanized surface was passivated with ethanolamine. Protein surface concentrations ranged from  $1.7 \text{ e-}13$  to  $2,73 \text{ e-}13 \text{ Mol/cm}^2$  for tumor necrosis factor- $\alpha$ , from  $1.6 \text{ e-}13$  to  $1.7 \text{ e-}13 \text{ Mol/cm}^2$  for the TNF- $\alpha$  antibody. In the PSA experiments surface concentrations ranged from  $1.6 \text{ e-}13$  to  $7.0 \text{ e-}13 \text{ Mol/cm}^2$  and from  $3.2 \text{ e-}13$  to  $6.1 \text{ e-}13 \text{ Mol/cm}^2$  for the PSA-antibody.

The validity of the antibody experiments was proved by determination of the binding ratios of antibody and antigen. The found ratios were 1.6 at maximum for tumor necrosis factor alpha and 3 to 5 for prostate specific antigen. In a final experiment a silicon MIRE was modified with aminopropyltrimethoxysilane (APTES). A sulfo-smcc crosslinker was bound to the surface and covalently connected with single-stranded DNA of 20 base-pairs. The complementary DNA strand was brought in contact to the resulting surface to mimic a DNA biosensor. Again it was tried to determine the surface concentrations of all involved molecules.

### **Zusammenfassung**

Biosensoren in Form von Nanodrähten, deren Basis in Kontakt mit der zu analysierenden Substanz steht, sind vielversprechende Werkzeuge, um Molekülkonzentrationen bis in den Femtomolarbereich zu bestimmen. FTIR-ATR Spektroskopie wurde verwendet, um Protokolle zur Oberflächenmodifikation sowie Möglichkeiten zur Proteinanbindung zu untersuchen. Die Einzelstrahl-Probe-Referenz Methode wurde verwendet, um Wasserabsorption, Lösungsmittelabsorption und Unregelmäßigkeiten in den verwendeten Mehrfachreflektionselementen zu kompensieren. In einen Schritt-für-Schritt Prozess wurden Mehrfachreflektionselemente aus Silizium und Germanium mit Silanen modifiziert sowie verschiedene Proteine angebunden, damit die Oberfläche einem Biosensor gleicht.

In einem Vorläuferexperiment wurde das Adhäsionsverhalten von Rinderserumalbumin (BSA) auf polierten und mit Silanen modifizierten Oberflächen studiert. In weiteren BSA Experimenten wurde die Oberflächenkonzentration unter

Einfluss von verschiedenen Kochsalzkonzentrationen gemessen. Die resultierenden Oberflächenkonzentrationen lagen zwischen  $1.5 \cdot 10^{-12}$  und  $2.4 \cdot 10^{-12}$  Mol/cm<sup>2</sup>. Anbindungsexperimente mit Protein-Ligand Systemen wie Streptavidin/Biotin, Tumornekrosefaktor- $\alpha$  (TNF- $\alpha$ ) und dessen Antikörper und Prostata-spezifisches Antigen (PSA) und dessen Antikörper wurden durchgeführt und die Oberflächenkonzentrationen bestimmt. Um unspezifische Adhäsion von Proteinen zu vermeiden, wurden die resultierenden Oberflächen mit Ethanolamin passiviert. Die Oberflächenkonzentrationen von TNF- $\alpha$  lagen zwischen  $1.7 \cdot 10^{-13}$  und  $2,73 \cdot 10^{-13}$  Mol/cm<sup>2</sup> und zwischen  $1.6 \cdot 10^{-13}$  und  $1.7 \cdot 10^{-13}$  Mol/cm<sup>2</sup> für den TNF- $\alpha$  Antikörper. In den PSA Experimenten lagen die Oberflächenkonzentrationen zwischen  $1.6 \cdot 10^{-13}$  und  $7.0 \cdot 10^{-13}$  Mol/cm<sup>2</sup>. Beim PSA Antikörper zwischen  $3.2 \cdot 10^{-13}$  und  $6.1 \cdot 10^{-13}$  Mol/cm<sup>2</sup>. Das Funktionieren der Antikörperexperimente wurde durch das Bestimmen der Bindungsverhältnisse bewiesen. Das Verhältnis für das Tumornekrosefaktor- $\alpha$  System war 1,6 und für das Prostata-spezifisches Antigen System war das Verhältnis 3 bis 5. In einem letzten Experiment wurde eine Mehrfachreflektionselement aus Silizium mit 3- Aminopropyltrimethoxysilan modifiziert, um anschließend einen sulfo-SMCC Linker anzubinden. An den Linker wurde eine 20 Basenpaare lange Einzelstrang-DNA gebunden und die Komplementärsequenz eingespült, um einen DNA-Biosensor darzustellen. Die resultierenden Oberflächenkonzentration aller verwendeten Substanzen wurden versucht zu messen.

## 1 Introduction

### 1.1 Biosensors

Biosensors are analytical devices designed to detect and transform the physicochemical signals of biological molecules into a machine readable electrical signal. Depending on the signal transformation the current biosensors are of the optical [1], nanomechanical [2-5], electrochemical or acoustic type [6, 7]. In recent years field-effect transistors have led to developments of devices called ion-selective field-effect transistors (ISFETs) [8-10]. The main difference of these devices compared to a standard metal-oxide semiconductor field-effect transistors (MOSFET) is the gate electrode. In ISFETs the gate lies bare to an aqueous solution, an additional electrode and an ion sensitive layer on the surface. This makes it possible to bring the gate into direct contact with the analyzable substances. Such ISFETs are mainly used to measure chemical parameters like ion concentrations or pH changes. The application of ISFETs led to the development of electrical field-effect transistors in the sub 1  $\mu\text{m}$  scale. These devices are also made of silicon and consist of a nanowire [11, 12] with a diameter of 50 – 100 nm and a drain and source electrode like a regular field-effect transistor. To achieve an effective gate a chemical and/or biological modification on the surface of the biosensor is necessary. The resulting modified devices can be used to detect biological and chemical compounds. These include immobilized antibodies [11, 13], DNA strands [14], streptavidin/avidin systems [15], diagnostically relevant species such as tumor markers [16], single nucleotide polymorphisms (SNPs) or screening

for viral or bacterial DNA. Advantages of this type of sensor include the high sensitivity and speedy detection results compared to more traditional methods like enzyme assays and diverse chromatographic approaches. The high sensitivity of nano field-effect transistor (nanoFET) is caused by its functionality as a variable current switch. This means a biological or chemical signal is also amplified while being transformed into an electrical signal. Additionally electrically charged molecules like proteins can cause a severe difference on the resulting electrical signal due to the extreme small scale construction of the device. This consequently leads a better signal to noise ratio of the sensor [17]. Most current devices are produced by semiconductor techniques on silicon which grants the possibility to use these devices with integrated circuitry. Furthermore the constant downsizing and further development of the biosensors led to label-free detection [18] of diagnostic markers from bodily fluids as their detection limits are into the fM range [19]. Cheap materials and the possibility of mass production of nanoFET biosensors created interest to gain a deeper insight into the physicochemical properties of the used materials and production processes. The constant miniaturization of the devices leads to problems due to material and manufacture limitations. Actual manufacturing processes result in devices, which give inconsistent signal responses. To safely use biosensors for diagnostic approaches the sensor signals must be uniform and predictable by mathematical models [20-22]. This work was prompted by researchers who were interested in the simulation modelling [23-25] of biosensor devices based on nanoFETs as no experimental data about surface concentrations were available of the molecules used so far in prototypes of nanoFETs.

## 1.2 Aim of this work and questions

In this work focus is laid upon some of the recent surface modification protocols and their applicability as well as the determination of concrete surface concentration values. Quantitative fourier-transformed infra-red (FTIR) attenuated total reflectance (ATR) spectroscopy was used for measuring molecular surface concentrations of functionalized surfaces similar to surfaces used in earlier experiments of prototypes of nanoFETs.

Initial questions were:

- Can the step by step procedure of the surface functionalization of a biosensor be mimicked and reproduced at various stages and adapted to fit adequate infrared measurements?
- What is the actual surface concentration of the diverse molecule-layers after the step-by-step manufacture process and what significance do changes in thermodynamic parameters during the functionalization have?
- What information can be gained on the feasibility and reproducibility of the current protocols?
- Can the bound molecules be feasibly detected?
- What stability does such a setup have?
- How do the results fit into already published information acquired by other methods?

### 1.3 Experimental strategy

In a first step of mimicking the processes of semi-conductor fabrication from monocrystalline silicon wavers, the same polishing procedure was applied to the silicon element of the IR-ATR measuring method.

Measurements were taken before and after experimenting with protein solutions and treating the silicon oxide surface with chemical modifications. After testing the surface to achieve information on the conformity of the polishing procedure a protein solution was applied on the silicon oxide surface to gain insight on the maximum possible coverage of a single protein monolayer.

Chemical modifications with silane linkers were applied to the polished silicon oxide surface with differing curing times and temperatures. A series of experiments was performed and all data from subsequent experiments was factored in to achieve information about the reproducibility of the aforementioned protocols.

After the fundamental step of silanisation, bonding experiments with proteins like BSA and streptavidin were conducted. BSA was used first, because it is well studied and inexpensive. Already available experimental data makes evaluation of the results considerably easier.

The well described streptavidin/biotin system promised to give good results in the spectroscopic measurements because of the high molecular weight of the avidin tetramer (MW = 4 x 66 kDa). Since an avidin molecule has 512 peptide bonds, a good signal-to-noise ratio can be achieved with more accurate results. Additionally biotin bonding experiments were performed on the protein layer to verify the viability of the system as a detector. Since the chemical structure of biotin enables the

possibility to bind it to a silane linker, a vice versa approach was tried with biotin attached to the surface. Every avidin molecule tetramer is able to bind 4 biotin molecules thus a determination of the binding ratios was tried.

In another experimental series anti-TNF- $\alpha$  antibodies were bound to the silane surface and subsequently brought into contact with its antigen tumor necrosis factor- $\alpha$  (TNF- $\alpha$ ). Bonding experiments with TNF- $\alpha$  were performed and surface concentrations and antibody/antigen ratios were determined.

A further series with focus on prostate-specific-antigen (PSA) and an appropriate antibody was conducted. Elevated PSA levels are an important diagnostic marker for prostate cancer thus improved detection systems are currently of high interest. Different concentrations of PSA antigen were tested and antibody/antigen ratios determined to test the limitations of a putative biosensor setup.

In a final experimental series the feasibility of short DNA strands bound to a silane linker molecule was tested. This biosensor setup raises possibilities to screen people for therapeutic benefit if the corresponding DNA sequences can be accurately detected. A bonding experiment with complementary DNA would highlight the differences between proteins and nucleic acids bound to the modified silicon oxide surface.

## 1.4 FTIR-ATR spectroscopy

When a beam of light penetrates optically transparent media (i.e. non absorptive) with different refractive indices the beam is both refracted and reflected. The reflected beam has the same angle as the incident beam of light.

The angle of the refracted beam can be calculated using Snell's law:

$$\frac{\sin(\theta_1)}{\sin(\theta_2)} = \frac{n_1}{n_2}$$

n ... refractive indices

$\theta$  ... angle of incidence

Total internal reflection (TIR) is a phenomenon taking place at the interface of a dense and a rare optical medium (e.g. glass and air). The incident light beam is not refracted anymore but instead totally reflected below the critical angle of incidence. The critical angle can also be calculated with Snell's law. At a closer look on the exact location of reflection a small distance between the incident and the reflected beam can be discerned. This shift was first described by Goos and Hänchen [26] in 1943. Since an electromagnetic wave cannot change its course abruptly, the beam dissolves into an evanescent wave which radiates into the rarer medium perpendicular to the interface. This effect is used in attenuated total reflection (ATR) spectroscopy by putting a sample substance on the surface of the denser medium. The evanescent wave will radiate from the denser medium into the sample.

Total internal reflection spectroscopy utilises the TIR phenomenon in an analysis method using infrared light to excite a sample substance at the interface of a denser, but transparent medium. The wavelength-dependence of the reflectivity of the interface is detected and recorded. The interaction of the evanescent wave with the sample material results in a substance-specific absorption spectrum. Especially thin layers can be investigated and the surface concentrations, molecular arrangement and functional groups of organic and biological molecules can be determined. To further enhance the signal-to-noise ratio Harrick [27] developed a multiple internal reflections method, which amplifies weak absorption signals. It utilizes a trapezoid shaped multiple internal reflection element mostly made of materials with high refractive indices in the infra-red range such as Germanium, Silicon and ZnSe.

Infra-red ranges below the wavelength of visible red light from 800 nm to 1000  $\mu\text{m}$  or 14000  $\text{cm}^{-1}$  to 10  $\text{cm}^{-1}$  in wave number notation ( $\tilde{\nu}=\lambda^{-1}$ ), which is preferred practice in infra-red spectroscopy and will always be used in this work. The measurements in this thesis were conducted in the mid infra-red region between 4000  $\text{cm}^{-1}$  and 400  $\text{cm}^{-1}$ , because the most relevant vibration patterns for the used chemical and biological materials are found in that wavelength range. The resulting spectra can be calculated [28] into surface concentrations values. All the above mentioned effects are combined into the FTIR-ATR measurement system used for almost all measurements in this thesis.

## **2 Methods and materials**

### **2.1 Chemicals used in this work**

#### **2.1.1 Bovine serum albumin**

Bovine serum albumin is one of the most used proteins in biological studies of model systems in science because it is inexpensive and easily acquired. Being a transport protein for various kinds of other molecules and ions it has a molecular weight of 66 kDa and consists of 583 amino acids. According to hydrodynamic data it is shaped like an ellipsoid with dimensions of 140 Å x 40 Å x 40 Å [29]. More recent data hint that BSA is shaped like human serum albumin in solution [30], which leads to a triangular shape of 80 Å x 80 Å x 80 Å x 30 Å. Because of its shape and profound adhesion behaviour [31] BSA is often used to achieve a tight monomolecular film. Solutions in a concentration range from 10 mM to 200 mM BSA were brought into contact with polished and modified silicon oxide surfaces under the regime of different salt and buffer concentrations as well as different treatment times. The resulting molecular density was measured.

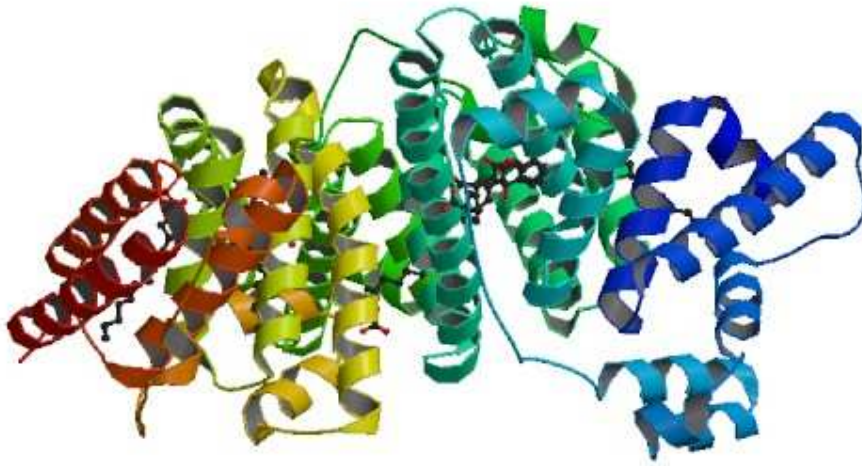


**Fig. 1. Ribbon model of bovine serum albumin.**

### **2.1.2 Tumor necrosis factor alpha (TNF- $\alpha$ )**

TNF- $\alpha$  is a protein molecule with therapeutic significance in Alzheimer's disease, inflammatory diseases and depression. It acts as cytokine signal molecule of immune cells and plays an important role in immune response and cancer development. TNF- $\alpha$  is a homotrimeric protein with a molecular weight of 52 kDa and consists of 486 amino acid residues. It is cone-shaped with a basal plane of approximately 24 nm<sup>2</sup> and a height of 5.5 nm.

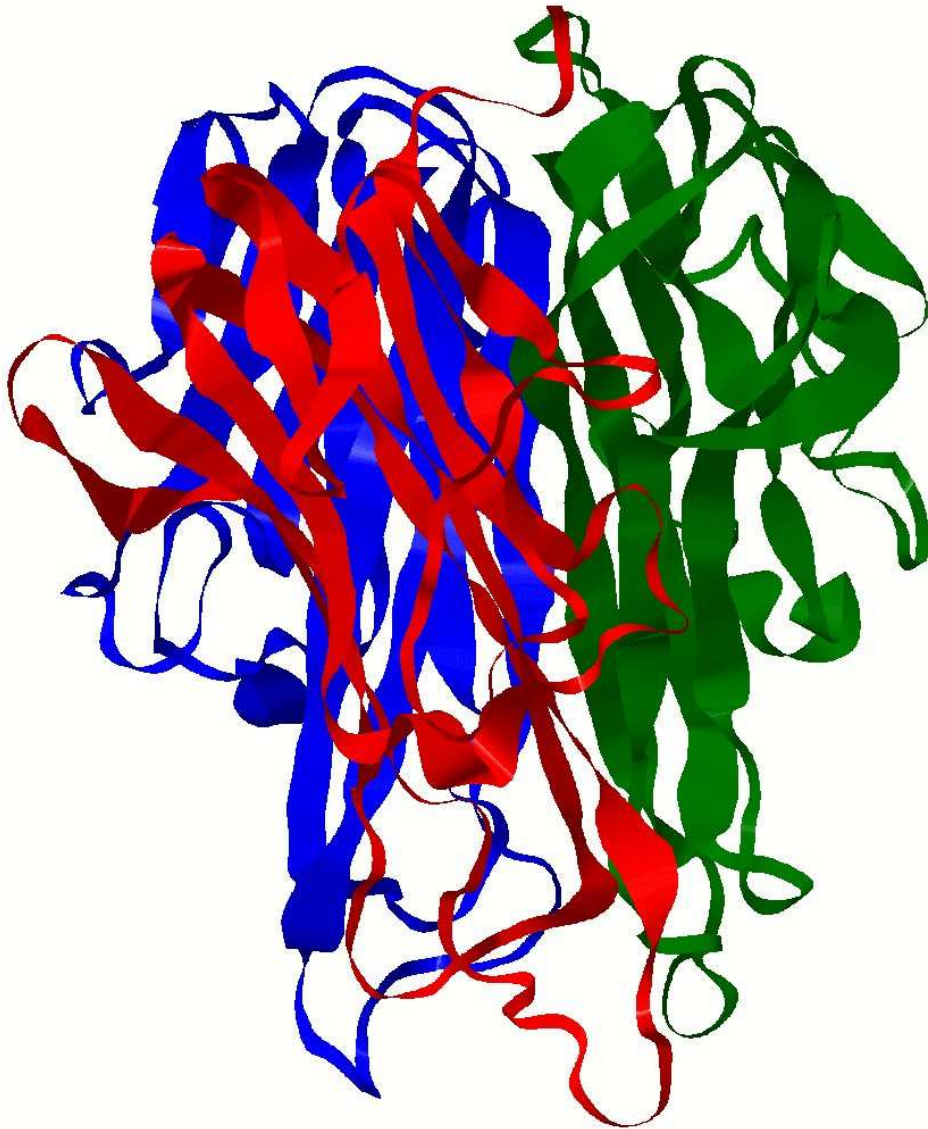


**Fig. 2. Ribbon model of tumor necrosis factor alpha [32].**

### **2.1.3 Prostate specific antigen (PSA)**

Prostate specific antigen also known as kallikrein-3 is produced by the epithelial cells of the prostate gland. Its primary function is the proteolysis of semenogelin and fibronectin in male seminal ejaculate. It also dissolves uterine mucus to enable spermatozoa to enter the uterus. PSA levels are elevated in men, who suffer from

prostate cancer, prostatitis and benign prostatic hyperplasia thus it became an important diagnostic marker for those medical conditions. It has a molecular weight of 32 kDa and consists of 236 amino acid residues.

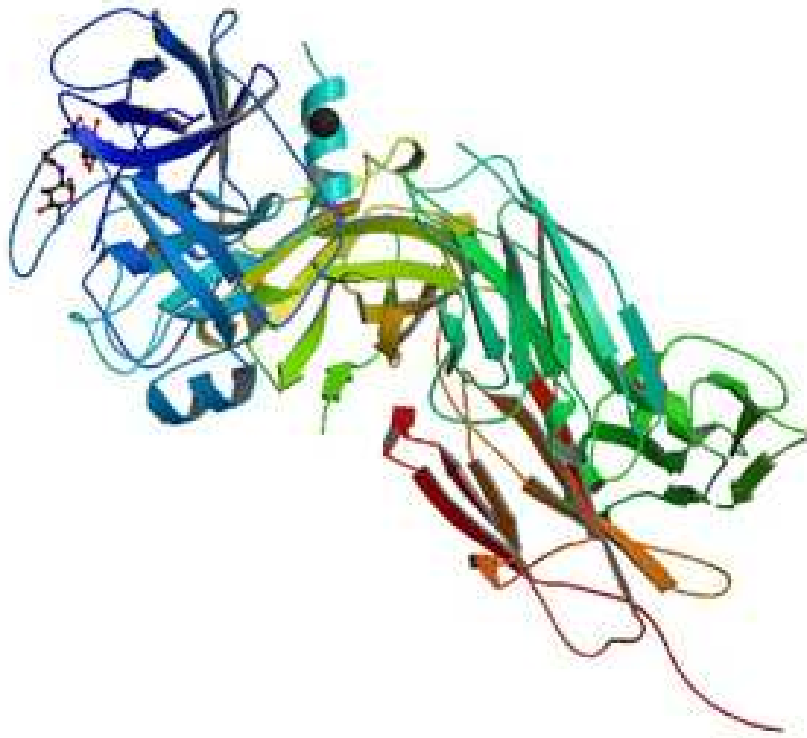


**Fig. 3. Ribbon model of prostate specific antigen [33].**

## **2.2 Multiple internal reflection elements (MIREs)**

To properly utilize the total internal reflection effect for spectroscopic measurements several conditions must be met. The material that brings sample and IR-light in contact must be optically transparent in the mid-IR range and of a sufficiently high refractive index to allow total internal reflection. Chemical inertness is also a highly

useful property as substances forming any kind of bond with the optic material will exhibit changed spectra, however with the methods in this work this change is utilized to gain quantitative information. Following this the most common materials for IR-spectroscopy are silicon, germanium and zinc selenide. Because higher numbers of active total reflections with the sample lead to higher absorption values and thus a better signal to noise ratio, a trapezoid shape has been devised as geometrical layout about 30 years ago. The IR-beam is aimed at the facets of the trapezoid and internally reflected several times depending on the length and height of the MIRE and the angle of incidence. The number of internal reflections can be thus calculated:

$$N = \frac{l}{w \cdot \tan \theta}$$

$l$  ... length of MIRE

$w$  thickness of MIRE

$\theta$ ... angle of incidence

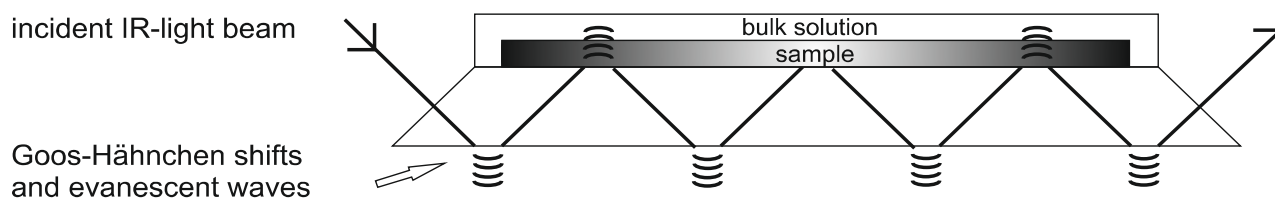


**Fig. 4. Cross-section view of multiple internal reflection element (MIRE). By putting a sample on the surface of an internal reflection element the sample substance comes into direct contact with the IR-light beam mediated by the evanescent waves. The resulting absorbance change is recorded and calculated into a spectrum.**

### 2.3 IR interaction with water

Water exhibits an unusually strong absorption for IR-light. The most significant vibration band is between 3800  $\text{cm}^{-1}$  and 3000  $\text{cm}^{-1}$  (stretching vibration). A second band has a maximum at 1640  $\text{cm}^{-1}$  (bending vibration). Since this is also the vibrational maximum of the amide I band, measurements in aqueous solution cannot account for solid information, because full compensation of the water bands is quite impossible. Because of these reasons only the amide II vibration with a maximum at 1540  $\text{cm}^{-1}$  was used for quantitative measurements and calculations in this work.

## 2.4 Calculation of the surface concentration [34]

The surface concentration  $\Gamma$  may be understood as the projection on the surface of the molecules in the volume defined by unit area and height  $d$  (real sample thickness). As a consequence, surface concentration of a thin layer can be determined without knowing the real thickness  $d$  and its real structure. The calculation is based on Lambert-Beer's law. For the ATR technique the introduction of the so-called "effective thickness"  $d_e$  first introduced by Harrick is required [27, 28, 35]. The volume concentration  $c$  and the surface concentration  $\Gamma$  are related to each other via the thickness  $d$  of the sample. By introducing Lambert-Beer's law one obtains

$$c = \frac{\Gamma}{d} = \frac{\int A_{pp|vp}(\tilde{\nu})d\tilde{\nu}}{N n d_{e,pp|vp}^{th} \int \varepsilon(\tilde{\nu})d\tilde{\nu}} \quad (3)$$

$\int A_{pp|vp}(\tilde{\nu})d\tilde{\nu}$  denotes the integrated absorbance of a distinct absorbance band measured with parallel (pp), or perpendicular (vp) polarized incident light, respectively.  $N$  is the mean number of the active internal reflections and  $n$  denotes the number of equal infra-red active groups per molecule leading to the absorbance of the evaluated bands.  $\int \varepsilon(\tilde{\nu})d\tilde{\nu}$  denotes the common integrated molar absorption coefficient of the vibrational mode of one infra-red active group.  $d_{e,pp|vp}^{th}$  is the effective thickness of the layer which depends on the polarization, the angle of incidence and the refractive indices of the MIRE and the sample.  $d_{e,pp|vp}^{th}$  is

regarding the theory of ATR the crucial value to be determined. In case of anisotropic samples (3) would lead to different results for parallel and vertical polarized light. Therefore the absorbance of both polarization directions has to be determined and to be considered in the calculation of the surface concentration using a model for the orientation of the molecules [28]. Here we used the model of liquid crystalline ultrastructure (LCU) for the calculation of surface concentrations. This model best fits the distribution of orientation of silanes and is also correct for isotropic distributions of molecules. For proteins the isotropic distribution was ensured by the determination of the dichroic ratio  $R_{exp.}$  (4) that has to be equal to the theoretical dichroic ratio  $R_{iso}^{th} = 1.6...$  valid for thin layers and the used optical parameters of ATR measurement.

$$R_{exp.} = \frac{\int A_{pp}(\tilde{\nu})d\tilde{\nu}}{\int A_{vp}(\tilde{\nu})d\tilde{\nu}} \quad (4)$$

As in the experiments with TNF- $\alpha$  the signal to noise ratio of the vp-measurements was very poor, the surface concentrations of TNF- $\alpha$  and its antibody were directly determined by the evaluation of (3) using results from pp measurements. The reader is referred to [27, 28, 35, 36] for more details of the quantitative evaluation of molecular surface densities using ATR technique. Optical parameters used in the calculations are  $45^\circ \pm 5^\circ$  angle of incidence, and refractive indices at wave number  $1540 \text{ cm}^{-1}$  for silicon ( $3.42 \pm 0$ ), germanium ( $4.01 \pm 0$ ), water ( $1.33 \pm 0.06$ ) and sample layer ( $1.45 \pm 0.06$ ). The number of active internal reflections was different in

different experiments and is given in table 2. Quantifications for all proteins were done by determining the absorbance of the amid II band that is only barely effected by uncompensated water absorbance. Nevertheless, the integrated absorbance was evaluated after compensation of the small negative water band at  $1640\text{ cm}^{-1}$  by adding an appropriate amount of a pure water spectrum. This negative absorbance leads from uncompensated water that was replaced after the measurement of the reference by the bound molecules of the investigated layer in the sample compartment and can therefore never be experimentally removed. The amount of added water absorbance was estimated by the remaining absorbance of the  $\text{H}_2\text{O}$  stretching vibration and by evaluating the ratio between integrated absorbencies of amid I and amid II vibrations. The resulting ratios were between 1.45 and 2.68 with a mean value of 2.25 for parallel polarized light and between 2.21 and 3.81 with a mean value of 2.63 for vertical polarized light. Estimated values of the error of integrated absorbencies are between 5 % and 30 % depending on the signal to noise levels of spectra and remaining uncompensated water absorption. All errors in the calculation of surface concentrations and dichroic ratios are evaluated using propagation of uncertainty.

## **2.5 SBSR measurement method**

To get the best possible compensation of water vapour and carbon dioxide the single-beam sample-reference method is used for this work [37]. It splits the MIRE into two lengthy flow-through compartments separated by o-rings made of viton. The

compartments are provided with tubings to attach pumps and additional tubes. A computer controlled stage lifts the MIRE in its compartments to the different sample and reference positions parallel to the IR-light beam. With this setup a good compensation of the solvent water can be achieved. The protein vibrations in this work are typically quantified according to their amide 1 (1640  $\text{cm}^{-1}$ ) and amide 2 (1540  $\text{cm}^{-1}$ ) bands and incompensations in that range will influence the results. Since IR-spectrometers have inhomogeneous intensity across their IR-beam a split of the beam would result in different intensities in the sample and reference compartments. Although this problem also exists in the SBSR method, it can be easily compensated by the proper adjustment of the mirrors. Even high quality MIREs have optical inhomogenities and so the optical path of the sample and the reference compartment will never be identical. To compensate for this an additional reference spectrum is always recorded prior to any surface modifications and included into the calculation of the final spectrum.

Peristaltic pumps are used to fill or rinse the compartments of the flow-through cell holding the MIRE to ensure the necessary accuracy for sensitive difference spectroscopy.

A proper container to hold a thin film of aqueous sample solution and the possibility to pump solutions in and out of the compartments is depicted in figure 5.



**Fig. 5. (left) Silicon ATR multiple internal reflection element (MIRE). (right) Teflon MIRE holder with fluid chambers, tubings and o-rings.**

## **2.6 Transmission spectrometer setup**

A Bruker IFS 25 FTIR spectrometer (Fig.6) with DTGS (deuterium tri-glycine sulphate) detector was used for the determination of the molar absorption coefficient. Transmission cells had about 100 $\mu$ l volume and the windows were made of calcium fluoride. The thickness of the mylar spacer was approximately 12 $\mu$ m. All FT-IR spectra were recorded at 4  $\text{cm}^{-1}$  resolution using Blackham-Harris 3-term apodization and a zero filling factor of 4. Interferograms were measured in single sided mode, which made phase correction using the Mertz function necessary. Dry air was constantly pumped into the measurement chamber to purge it from water vapour and carbon dioxide.

## 2.7 IR-ATR spectrometer setup

In this thesis the most important measuring device is the Bruker IFS 66 spectrometer set up on an optical table (Fig. 6). To record the spectra a MCT (mercury – cadmium – telluride) detector cooled with liquid nitrogen is used. The polarisation of the incident IR-beam is done via an aluminium grid polarizer on a KRS-5 substrate (Specac, Orpington, U.K.). All multiple internal reflection elements (MIRE) are made of Silicon and Germanium and have a trapezoidal shape with dimensions of 52 x 20 x 1,5 mm (length x width x thickness). The IR-beam's angle of incidence  $\Theta$  was set at 45° for all experiments. All FT-IR spectra were recorded at 4 cm<sup>-1</sup> resolution using Blackham-Harris 3-term apodization and a zero filling factor of 4. Interferograms were measured in double sided mode. The spectrometer was constantly purged with dry and carbon dioxide free air. Flow-through cells made of Delrin® were used to fixate the MIREs. These cells allow to pump different solutions into the MIRE-chamber while keeping air-bubbles out of the system which lead to severe incompensations and make the results useless. Attached water circulation tubing makes it possible to thermostate the flow-through cell or perform necessary temperature changes.



**Fig. 6. (left) IFS 66 spectrometer with detector (red) and attached peristaltic pumps. (right) IFS 25 spectrometer. (bottom) schematics of an FTIR-ATR spectrometer.**

## **2.8 Determination of molar absorption coefficient of 3-trimethoxysilylbutyl aldehyde**

### **Materials**

Nitric acid 69% (Sigma-Aldrich), absolute ethanol for spectroscopy (Fluka), 3-(trimethoxy)butylsilyl aldehyde (UCT, Bristol), IFS 25 spectrometer (Bruker Electronics, Switzerland), PM-5 polishing machine (Logitech, Scotland), plasma cleaner (Harrick Sci corp) PTFE syringe filters 20 $\mu$ m cut-off (Sartorius, Germany), calcium fluoride transmission cell.

In order to accomplish the calculation of any surface concentration it is necessary to know the molar absorption coefficient of the substance. This measurement is done in transmission IR-spectroscopy using the IFS-25 device by Bruker Electronics. A calcium fluoride ( $\text{CaF}_2$ ) cell with a 25  $\mu\text{m}$  Teflon spacer was used.

To determine the exact thickness of the liquid layer in the transmission measurement cell the so called “fringe-method” was used. Fringes are caused by the difference in refraction indices of the liquid layer and the window material of the cell. By measuring the wave number differences of fringe maxima or minima of an empty cell, the layer thickness can be calculated with following equation [38]:

$$b = \frac{m}{2} \frac{1}{\nu_1 - \nu_2} [\text{cm}]$$

b ... thickness of liquid layer

m ... number of fringes

$\nu_1$  ... lower wave number limit

$\nu_2$  ... higher wave number limit

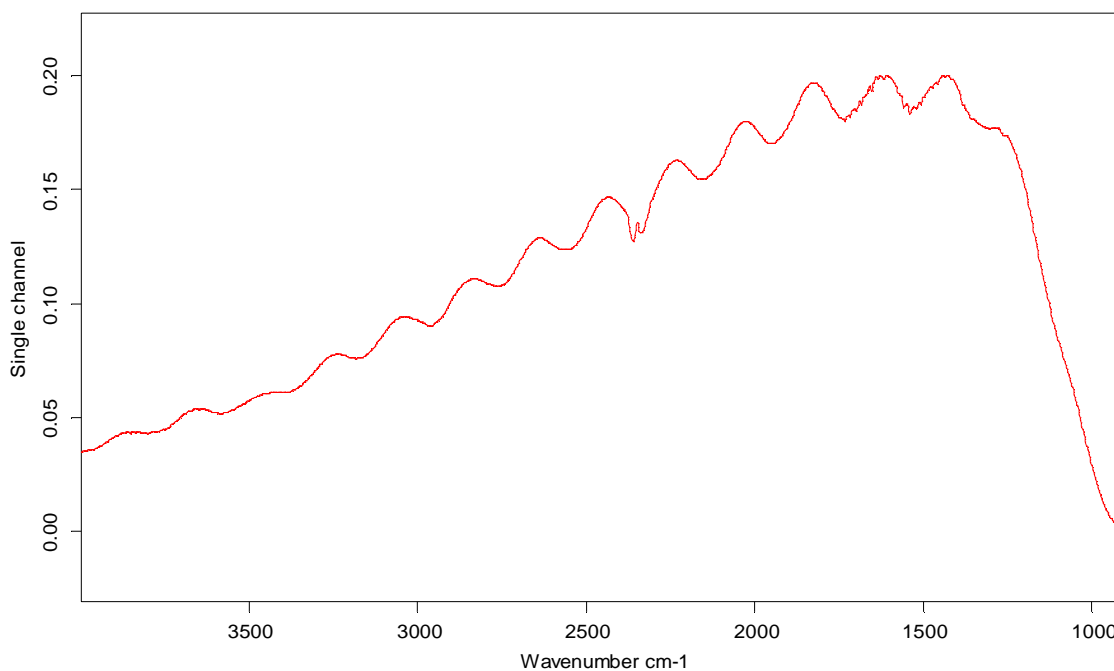


**Fig. 7. Single channel transmission spectrum of an empty CaF<sub>2</sub> transmission cell. Several fringes are visible. The negative bands at 2300 cm<sup>-1</sup> are caused by the CO<sub>2</sub> stretching vibration. The whole cell cuts-off signal at 1000 cm<sup>-1</sup>.**

3-trimethoxysilylbutyl aldehyde is solved in 96% EtOH and a concentration series is established.

The average value in the following table is used for surface concentration calculations.

<b>experiment</b>	<b>coefficient</b>
no.1	829693 cm/Mol
no.2	888966 cm/Mol
no.3	869062 cm/Mol

<b>average</b>	<b>862574 cm/Mol</b>
standard deviation	30164 3,5 %

## 2.9 Preparation of silicon ATR-elements

Since it was important to create the same polished surface on the silicon ATR element as in the semiconductor industry the same tools were used. The polishing machine was a Logitech PM-5, the polishing cloth was made of polyurethane and a Logitech SF-1 polishing liquid was used (alkaline colloidal silica). The trapezoid shaped ATR-elements were polished on both sides for 20 min at a rotation speed of 60 rpm. Investigations by microscope showed a scratch less surface compared to a standard polishing method with diamond polishing paste of 0,25  $\mu\text{m}$  grain-size. After polishing the element is cleaned with acetone, water and ethanol to remove any traces of polishing suspension and fixing wax. To remove any metal ions from the surface that could possibly interfere with the silanisation process the MIRE is attached to a Teflon holder and refluxed for 4 h in 70% nitric acid.

**For lab security reasons it was made sure to remove any ethanol from the element before refluxing it in highly concentrated nitric acid!**

As a final preparation step, a 3 min plasma clean is done.

2.10 Schemes of silane modifications

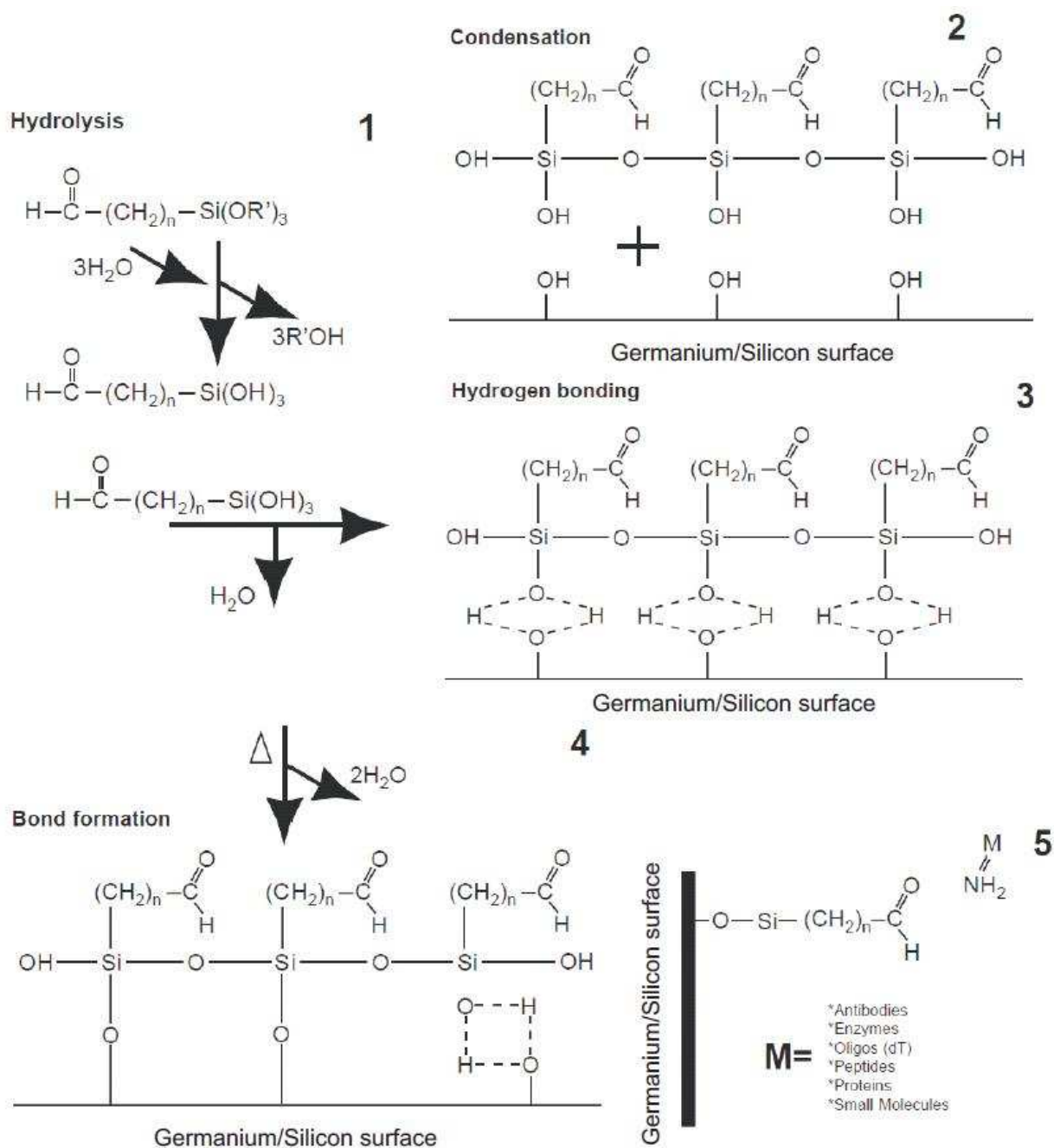


Fig. 8. Reaction scheme for surface modification by deposition of 3-trimethoxysilylbutyl aldehyde. Step 1 shows hydrolysis of single silane

molecules. Step 2 shows the condensation reaction between several silane molecules resulting in a chain-like structure. Step 3 details the formation of hydrogen bonds between the silane chain and the surface. In step 4 the application of heat leads to covalent bonds. Step 5 describes the possible modifications of the aldehyde silane with amino-group containing molecules.

### **2.11 Experimental procedure for silanisation of silicon ATR-elements using 3-(trimethoxy) butylsilyl aldehyde**

#### **Materials**

Nitric acid 69% (Sigma-Aldrich), absolute ethanol for spectroscopy (Fluka), 3-(trimethoxy) butylsilyl aldehyde (UCT, Bristol), IFS 66 spectrometer (Bruker Electronics, Switzerland), PM-5 polishing machine (Logitech, Scotland), plasma cleaner (Harrick Sci corp) PTFE syringe filters 20µm cut-off (Sartorius, Germany)

According to the protocol of Patolsky et al. [11] following adapted procedure has been performed:

- Prepare properly polished and cleaned silicon MIRE
- Prepare solution of 1% 3-(trimethoxy) butylsilyl aldehyde in 96% EtOH
- Filter solution with a 20 µm cut-off PTFE syringe filter
- Pump silane solution into the sample-compartment of the flow-through cell

- Reaction time is 30 min. The silane forms hydrogen bonds with the silanol groups (SiOH) of the silicon surface according to Fig.5.
- Slowly pump out solution (2  $\mu$ l/s flow speed)
- Rinse the sample-compartment with 96% EtOH to flush out any unbound silane
- Apply heat to the flow-through cell for 30 mins. For technical reasons a temperature of 80°C is chosen for the silanisation instead of the 120°C stated in the protocol by Patolsky et al. Measurements show this does not decrease the silanisation efficiency and resulting surface concentration of covalently bound silane (see Results). This step forms covalent bonds between the silane and the silanol surface.
- Cooldown phase. Drop temperature from 80°C to 25°C .
- Rinse flow-through cell thoroughly with 96% EtOH to remove any non-covalently bound silane from the surface.
- Measurement and quantification

## **2.12 Passivation of silane aldehyde surface**

It was not predicted for most proteins to form a monolayer on the aldehyde surface or completely block off all aldehyde moieties. Thus after protein binding, any remaining CHO-groups must be capped to prevent any unspecific binding, especially in anti-body experiments.

- Rinse sample compartment with a solution of 100 mM ethanolamine in phosphate buffer pH 8.4 and 4 mM cyanoborohydride. It uses the same reaction mechanism described above in the protein binding section.
- Wait 2 h.
- Rinse sample-compartment with phosphate buffer.
- Measurement and calculation

### 2.13 BSA saturation experiments

#### Materials

Bovine serum albumine (Sigma-Aldrich), di-sodium hydrogen phosphate dihydrate (Merck, Darmstadt), sodium dihydrogen phosphate anhydrous (Fluka), potassium dihydrogen phosphate (Fluka), nitric acid 69% (Sigma-Aldrich), absolute ethanol for spectroscopy (Fluka), 3-(trimethoxy)butylsilyl aldehyde (UCT, Bristol), IFS 66 spectrometer (Bruker Electronics, Switzerland), PM-5 polishing machine (Logitech, Scotland), plasma cleaner (Harrick Sci corp) PTFE syringe filters 20 $\mu$ m cut-off (Sartorius, Germany). The following buffer solutions were prepared: 10mM phosphate (potassium salts) at pH 7.4 with additional 2 $\mu$ M KCl, 10mM phosphate (potassium salts) at pH8.4. Ethanol solutions of 96% were prepared with spectroscopic ethanol and ultrapure water. All solutions were degassed prior to use.

## 2.14 Experimental procedures for BSA saturation experiments

To test for a full surface coverage a BSA experiment series has been done. Three experimental series have been done on non-modified MIREs:

- 1) bare silicon surface
- 2) bare germanium surface
- 3) bare silicon surface with additional sodium chloride

- The MIRE was rinsed with buffer solution. Care must be taken to not bring any air-bubbles into the tubing system.
- A reference spectrum of both compartments is taken.
- The MIRE is rinsed with a solution of 100 mM BSA in phosphate.
- Wait for 1 h to let proteins attach to the surface. A measurement is taken in that time to confirm the filling of the sample-compartment with protein solution.
- Rinse for 10 min with buffer solution.
- Take measurement.
- Repeat at step 3 (rinse with phosphate buffer) to create a series of protein binding events for the experiments.

Another experiment tests the possibility to influence the surface coverage with a raising sodium chloride concentration in the buffer. The used concentrations ranged from 0 mM to 200 mM NaCl.

## 2.15 Protein binding to silan aldehyde surface

The proteins used in these experiments are either reconstituted or diluted in 10 mM sodium or potassium phosphate buffer with a pH of 8.4 additionally containing 4 mM sodiumcyanoborohydride ( $\text{NaCNBH}_3$ ) to reduce the Schiff's bases to amide bonds.

### 2.15.1 Experimental procedures for the biotin/streptavidin system

#### Materials

Di-sodium hydrogen phosphate dihydrate (Merck, Darmstadt), sodium dihydrogen phosphate anhydrous (Fluka), potassium dihydrogen phosphate (Fluka), nitric acid 69% (Sigma-Aldrich), absolute ethanol for spectroscopy (Fluka), 3-(trimethoxy)butylsilyl aldehyde (UCT, Bristol), IFS 66 spectrometer (Bruker Electronics, Switzerland), PM-5 polishing machine (Logitech, Scotland), biotin (Sigma-Aldrich), streptavidin (Sigma-Aldrich), plasma cleaner (Harrick Sci corp) PTFE syringe filters 20 $\mu\text{m}$  cut-off (Sartorius, Germany). The following buffer solutions were prepared: 10mM phosphate (potassium salts) at pH 7.4 with additional 2 $\mu\text{M}$  KCl, 10mM phosphate (potassium salts) at pH8.4. Ethanol solutions of 96% were prepared with spectroscopic ethanol and ultrapure water. All solutions were degassed prior to use.

- Prepare a silanised silicon MIRE
- Take a reference measurement of both compartments

- Prepare solution of 200 µg/ml Streptavidin in 10 mM Phosphate buffer and 4 mM cyanoborohydride
- Pump protein solution into sample-compartment
- Let reaction occur for 1,5 h while recording a fill-spectrum
- Rinse the sample-compartment with buffer
- Measurement
- Rinse with passivation solution (see below)
- Wait for 60 min
- Rinse with buffer
- Measurement
- Rinse with biotin solution (5x biotin to streptavidin)
- Measurement

### 2.15.2 Experimental procedures for hTNF- $\alpha$ antibody and antigen system

A surface with anti-TNF- $\alpha$  antibody is prepared and a concentration series of its antigen TNF- $\alpha$  is done.

#### Materials

Di-sodium hydrogen phosphate dihydrate (Merck, Darmstadt), sodium dihydrogen phosphate anhydrous (Fluka), potassium dihydrogen phosphate (Fluka), nitric acid 69% (Sigma-Aldrich), absolute ethanol for spectroscopy (Fluka), 3-

(trimethoxy)butylsilyl aldehyde (UCT, Bristol), IFS 66 spectrometer (Bruker Electronics, Switzerland), PM-5 polishing machine (Logitech, Scotland), monoclonal hTNF- $\alpha$  antibody (Center for Biomedical Technology, Danube University, Krems, Austria), human TNF- $\alpha$  (Stratham Biotec AG), plasma cleaner (Harrick Sci corp) PTFE syringe filters 20 $\mu$ m cut-off (Sartorius, Germany). The following buffer solutions were prepared: 10mM phosphate (potassium salts) at pH 7.4 with additional 2 $\mu$ M KCl, 10mM phosphate (potassium salts) at pH8.4. Ethanol solutions of 96% were prepared with spectroscopic ethanol and ultrapure water. All solutions were degassed prior to use.

- Prepare a silanised silicon MIRE
- Take a reference measurement of both compartments
- Prepare solution of 100  $\mu$ g/ml anti-hTNF- $\alpha$  in 10 mM phosphate buffer and 4 mM cyanoborohydride
- Pump protein solution into sample-compartment
- Let reaction occur for 2 h while recording a fill-spectrum
- Rinse the sample-compartment with buffer
- Measurement
- Fill with passivation solution (see below)
- Wait for 60 min
- Rinse with buffer
- Measurement
- Fill sample-compartment with hTNF- $\alpha$  solutions (1  $\mu$ g/ml) and let stand for 2h
- Measurement

- Rinse sample-compartment with buffer to remove superfluous protein
- Measurement
- Repeat the above steps with hTNF- $\alpha$  solutions 5  $\mu\text{g/ml}$ , 10  $\mu\text{g/ml}$  and 18  $\mu\text{g/ml}$

### 2.15.3 Experimental procedures for the PSA-antibody and PSA system

#### Materials

Di-sodium hydrogen phosphate dihydrate (Merck, Darmstadt), sodium dihydrogen phosphate anhydrous (Fluka), potassium dihydrogen phosphate (Fluka), nitric acid 69% (Sigma-Aldrich), absolute ethanol for spectroscopy (Fluka), 3-(trimethoxy)butylsilyl aldehyde (UCT, Bristol), prostate-specific antigen antibody (Fisher Scientific), prostate specific antigen (Calbiochem), IFS 66 spectrometer (Bruker Electronics, Switzerland), PM-5 polishing machine (Logitech, Scotland), plasma cleaner (Harrick Sci corp) PTFE syringe filters 20 $\mu\text{m}$  cut-off (Sartorius, Germany). The following buffer solutions were prepared: 10mM phosphate (potassium salts) at pH 7.4 with additional 2 $\mu\text{M}$  KCl, 10mM phosphate (potassium salts) at pH8.4. Ethanol solutions of 96% were prepared with spectroscopic ethanol and ultrapure water. All solutions were degassed prior to use.

- Prepare a silanised silicon MIRE
- Take a reference measurement of both compartments
- Prepare solution of 50  $\mu\text{g/ml}$  anti-PSA mouse antibody in 10 mM phosphate buffer pH 8.4 and 4 mM cyanoborohydride

- Pump protein solution into sample-compartment
- Let reaction occur for 2 h while recording a fill-spectrum
- Rinse the sample-compartment with buffer pH 7.4
- Measurement
- Fill with passivation solution (see below)
- Wait for 60 min
- Rinse with buffer pH 7.4
- Measurement
- Fill sample-compartment with PSA solution (0.5  $\mu\text{g/ml}$ ) in phosphate buffer pH 7.4
- Wait for 2h and take a measurement
- Rinse sample-compartment with buffer to remove superfluous protein
- Measurement
- Repeat the above steps with hTNF- $\alpha$  solutions 1  $\mu\text{g/ml}$ , 2  $\mu\text{g/ml}$ , 3  $\mu\text{g/ml}$  5  $\mu\text{g/ml}$ , 10  $\mu\text{g/ml}$  and 23  $\mu\text{g/ml}$ .

### **2.16 Experimental procedures for DNA-recognition system**

The procedures were adapted from protocols of Eric Stern's doctoral thesis and other publications [39, 40]. A cross-linker system was established in a step-to-step procedure with attached ss-DNA as final surface. Complementary DNA was then tested on the resulting surface. The reaction scheme is found in following Figure:

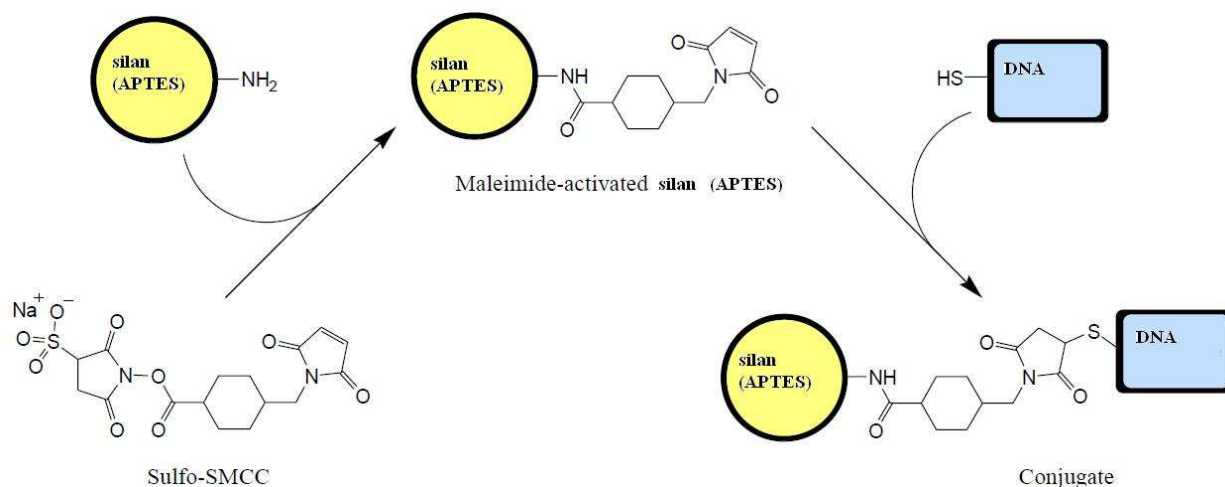


**Fig. 9. Reaction scheme of sulfo-smcc on an amino terminated surface. In a second step the sulfhydryl-group of the DNA 20-mer is bound to the cross-linker.**

## Materials

Di-sodium hydrogen phosphate dihydrate (Merck, Darmstadt), sodium dihydrogen phosphate anhydrous (Fluka), potassium dihydrogen phosphate (Fluka), nitric acid 69% (Sigma-Aldrich), absolute ethanol for spectroscopy (Fluka), 3-(trimethoxy)butylsilyl aldehyde (UCT, Bristol), IFS 66 spectrometer (Bruker Electronics, Switzerland), PM-5 polishing machine (Logitech, Scotland), plasma cleaner (Harrick Sci corp) PTFE syringe filters 20 $\mu$ m cut-off (Sartorius, Germany), hexane (Sigma-Aldrich). Sensor DNA: C6-5'- CCT GCA GTG ACG CAG TGG CG -3', Target DNA: 3'-GGA CGT CAC TGC GTC ACC GC -5'-C6. The following buffer solutions were prepared: 10 mM TE buffer at pH 7.5 for the sensor DNA attachment. 10 mM Tris + 1 mM EDTA + 50 mM NaCl at pH 7.5 as annealing buffer for the target DNA. All solutions were degassed prior to use.

- Prepare properly polished and cleaned silicon MIRE
- Prepare solution of 1% APTES in hexane
- Filter solution with a 20 µm cut-off PTFE syringe filter
- Pump silane solution into the sample-compartment of the flow-through cell
- Reaction time is 90 min.
- Slowly pump out solution (2 µl/s flow speed)
- Rinse the sample-compartment with hexane to flush out any unbound silane
- Apply 80°C of temperature to the flow-through cell for 120 mins.
- Cooldown phase. Drop temperature from 80°C to 25°C .
- Rinse flow-through cell thoroughly with hexane to remove any non-covalently bound silane from the surface.
- Measurement and quantification
- Prepare solution of 0,75 mg/ml sulfo-smcc
- Pump above solution into sample-compartment
- Measurement
- Wait for 30 mins
- Rinse sample-compartment with 10 mM TE buffer pH 7.5
- Prepare solution of 800 µg/ml sensor DNA in 10 mM TE buffer at pH 7.5
- Pump DNA solution into sample-compartment
- Wait for 1 h
- Rinse sample-compartment with annealing buffer
- Prepare solution of target-DNA. Concentration is 880 µg/ml
- Pump Target DNA solution into sample-compartment
- Wait 2 h for annealing to complete

- Rinse with annealing buffer
- Measurement

### 3 Results and Discussion

#### 3.1 Surface concentration of 3-(trimethoxy)butylsilyl aldehyde

The first chemical modification step to get a protein covalently bound to a silicon surface is the application of a linker molecule. In this case 3-(trimethoxy)butylsilyl aldehyde. A protocol of Patolsky et al. [11] was adapted to suit the needs of the IR-ATR technique and to receive reproducible surface concentrations of the silane.

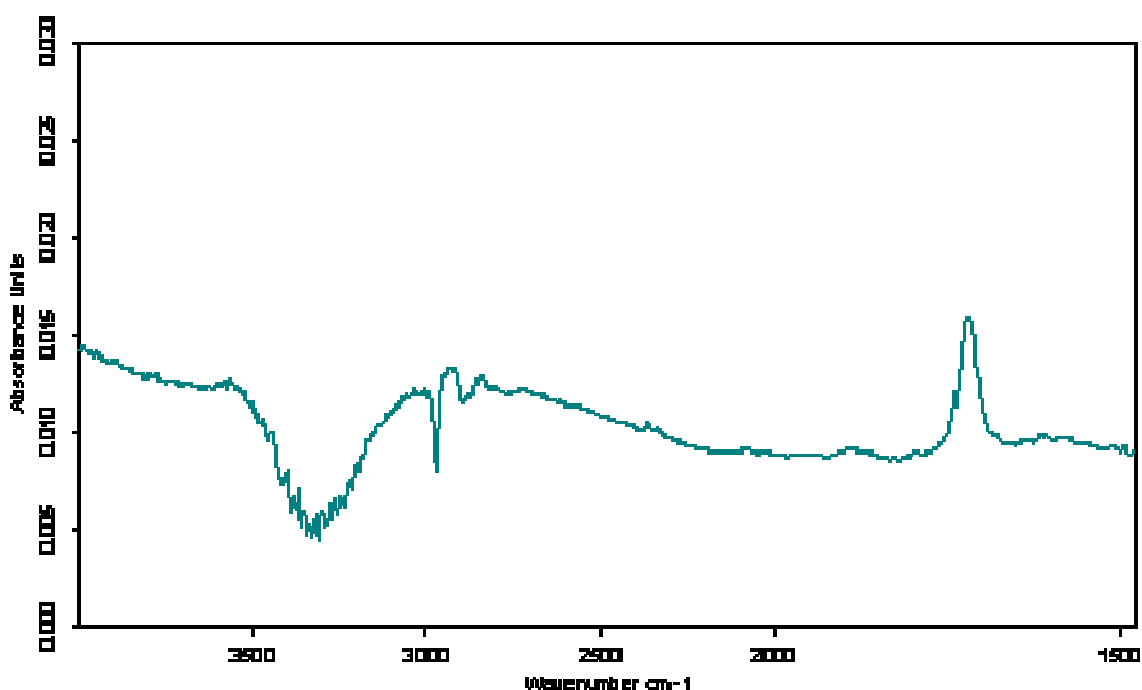
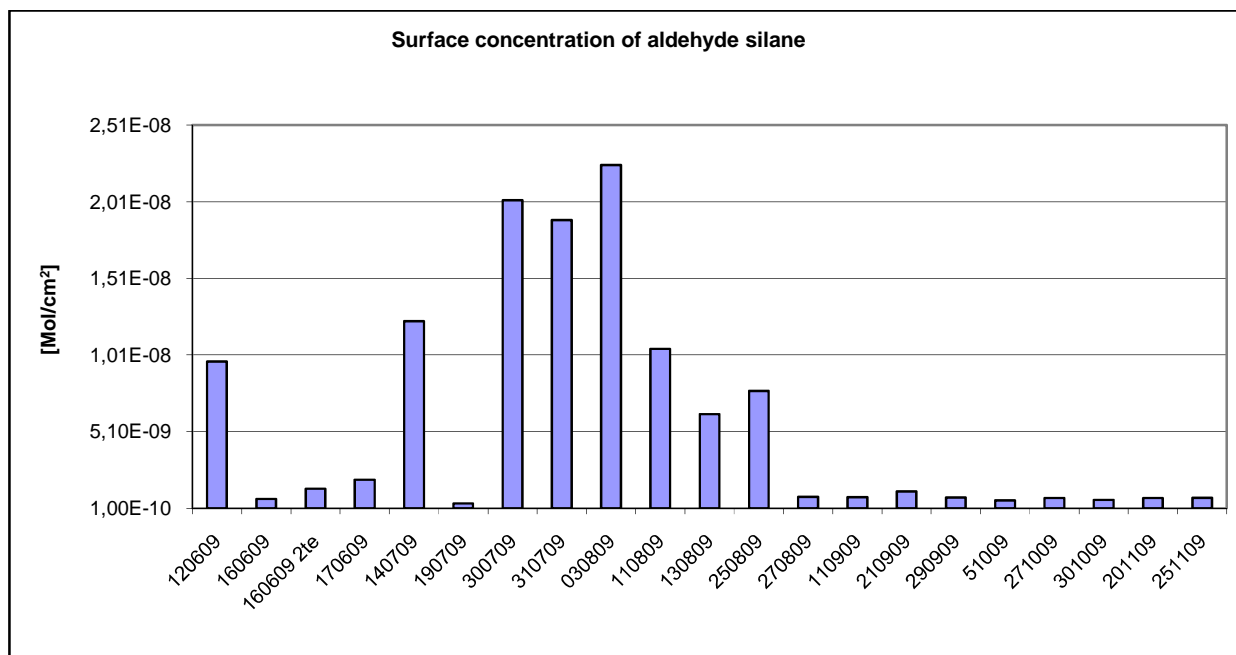


Fig. 10. FTIR-ATR absorbance spectrum of 3-(trimethoxy)butylsilyl aldehyde on silicon (compressed wavenumber display). The quantitatively evaluated band is the C=O (carbonyl) vibration of the tail-group of the used silane (see for structure) at  $1720\text{ cm}^{-1}$ . It indicates free carbonyl groups of silane on the

silicon surface ready to form imine bonds with amino-groups of proteins. Other bands are caused by EtOH and H<sub>2</sub>O incompenations despite the SBSR measurement method.



**Fig. 11. Series of silanisation experiments on silicon. Results vary significantly depending on the details of the silanisation protocol. Starting with the experiment on 27th of August the surface concentrations stays roughly the same after setting up a proper experimental protocol. The surface concentrations of the final experiments vary between 6,00 e-10 Mol/cm<sup>2</sup> and 1,20 e-9 Mol/cm<sup>2</sup>.**

Quantification was done by integrating the absorbance of the C=O-vibration at 1720 cm<sup>-1</sup>. The measured surface concentrations with optimized protocols for silanisation are between 6,00 e-10 Mol/cm<sup>2</sup> and 1,20 e-9 Mol/cm<sup>2</sup>. An estimated monolayer was

calculated using simple geometrical considerations (square sections). The required area for a single silane molecule is about  $0,25 \text{ nm}^2$ . This results in a theoretical surface concentration value of  $6,64 \text{ e-}10 \text{ Mol/cm}^2$  for an estimated monolayer.

The basic silanisation experiments showed extremely inconsistent results. The extreme differences in surface concentrations was most likely caused by the nano-scale surface roughness of the ATR-element resulting in a larger surface area than theoretically estimated by simple geometrical calculations of the area. This was partly overcome by the refined polishing process with polyurethane cloth and silica suspension. The results of Matijăsević [41] gave a surface concentration of  $6,33 \text{ e-}10 \text{ mol/cm}^2$  [42] for 7-OCTS. Theoretical area considerations gave  $0,34 \text{ nm}^2$  per silane molecule. Melnikoff [43] reports a surface concentration of  $2,95 \text{ } \mu\text{mol/m}^2$  for APDME, which is  $2,95 \text{ e-}10 \text{ mol/m}^2$ . These results are consistent with the results in this work.

Other scientists experienced problems with the polymerisation process of trimethoxy silanes, which is fast but can lead to different chain lengths and clusters of silane molecules. The usage of ethoxy silanes can be an improvement to prevent the formation of silane clusters at the cost of longer reaction times and more complicated reaction environments. The most important change of the original silanisation protocol is a 4 h boiling step in 70% nitric acid. This activates the surface and removes any metal cations, which interfere with the silanisation process. This so called leeching process led to stable and reproducible surface concentration values.

Keeping a strict experimental checklist as well as relying on automation like programmable pumps and using software macros was mandatory for reproducible results. It proved best to minimize human interaction to prevent resulting experimental mistakes.

### 3.2 Surface concentrations of BSA on blank silicon and germanium surfaces

Three experiment series were conducted. The first series with Germanium as ATR-element material. A second series on silicon without any additional sodium chloride. Experiment series number three on silicon with 200mM NaCl added to the buffer.

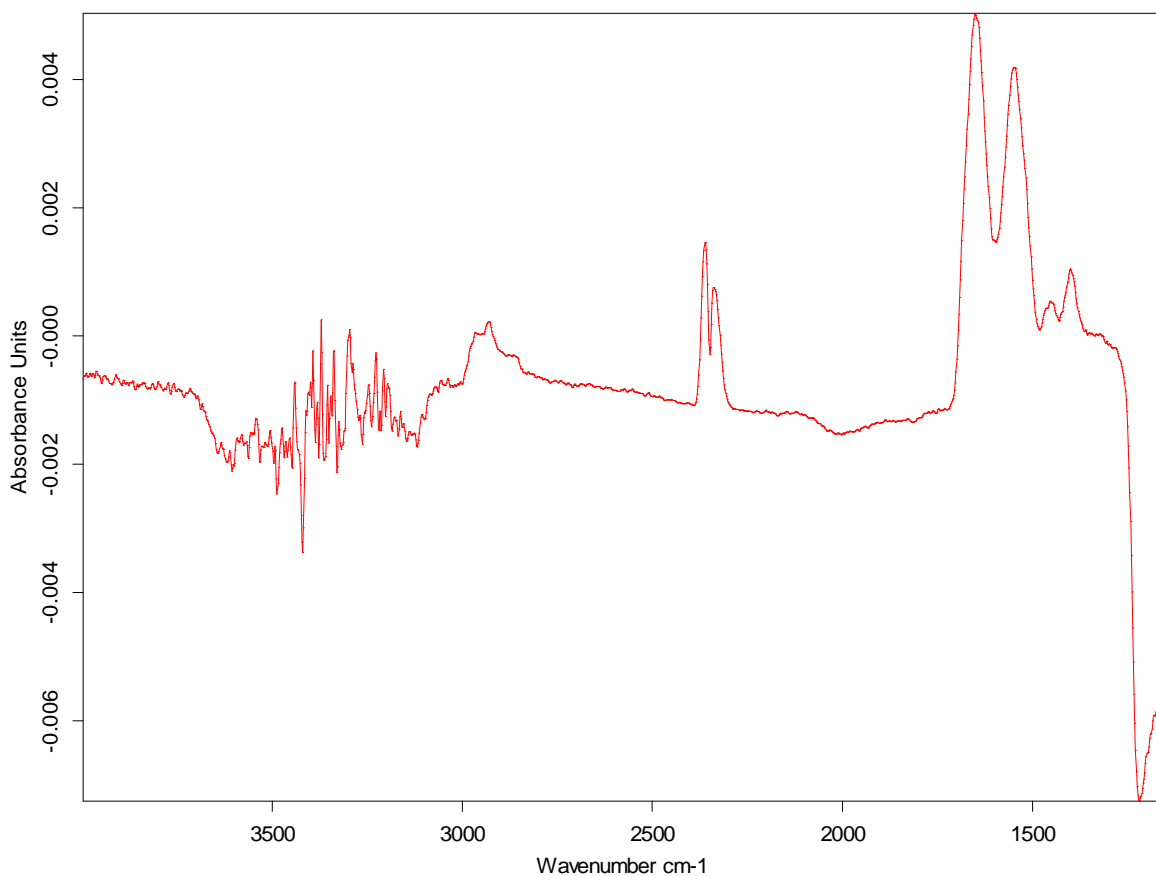


**Fig. 12. FTIR-ATR absorbance spectrum of BSA on silicon. The quantitatively evaluated vibration is the amide 2 bond at  $1540\text{ cm}^{-1}$ . Additionally the CH<sub>2</sub> vibrations from 2980 to 2830  $\text{cm}^{-1}$  are visible. Water and CO<sub>2</sub> incompenations are at 3400  $\text{cm}^{-1}$  and 2600  $\text{cm}^{-1}$  respectively. The large negative peak at 1200  $\text{cm}^{-1}$  is caused by the wave length cut-off of the silicon MIRE.**

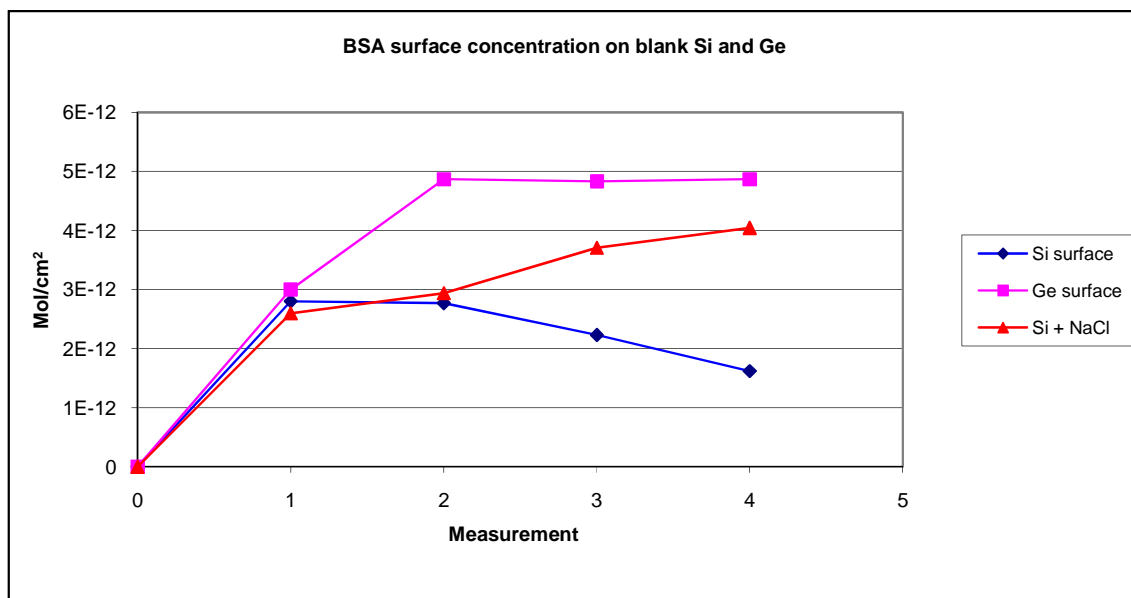


**Fig. 13. Comparison of BSA surface concentrations on Germanium and Silicon surfaces resulting in protein concentrations of 25mg/ml. Protein solution was allowed to adsorb for 2h before each measurement. Protein concentrations are generally higher on Germanium than on Silicon, until the addition of NaCl to the buffer lead to increased surface concentrations on Silicon. All measurements were done subsequently.**

BSA concentrations in the first experiment series maximized at almost  $5,0 \text{ e-}12 \text{ Mol/cm}^2$  after the second measurement. This value corresponds well with measurements done by Hassler [44], who determined a value of  $5,7 \text{ e-}12 \text{ Mol/cm}^2$  on a Germanium surface. On silicon the maximum surface concentration value achieved is  $4,0 \text{ e-}12 \text{ Mol/cm}^2$ . Without any added sodium chloride the achievable concentrations are  $2,8 \text{ e-}12 \text{ Mol/cm}^2$ .

The maximum achievable protein surface concentrations had to be estimated, because a working biosensor should best have a uniform monolayer. Any blank silicon surfaces can unspecifically bind other proteins, for instance blood albumins. The electric charge of the molecules would lead to a signal distortion in the electronic read-out. The germanium surface was tested to receive comparable results to the work of Hassler [44], who achieved  $5,7 \text{ e-}13 \text{ Mol/cm}^2$ . Since these results were quite consistent, silicon was tried. On silicon surfaces sodium chloride was added to the buffer solution, which led to higher surface concentrations of protein ( $4,0 \text{ e-}12 \text{ Mol/cm}^2$ ) compared to the blank surface ( $2,8 \text{ e-}12 \text{ Mol/cm}^2$ ). The higher ionic strength is capable of masking electrical charges on the silicon surface [45] resulting in a higher surface concentration. But since high salt concentrations cannot be used in a real nanosensor setup, because of the increased conductivity of the system, the attachment of the proteins to the aldehyde silane linker probably achieves the desired monolayer.

### **3.3 Bovine serum albumin (BSA) on aldehyde silane layer**

To get more insight on the protein adhesion and binding properties of a silanised surface and how it effects the surface concentration, a comparison experiment between a silanised and a non-silanised surface was done.

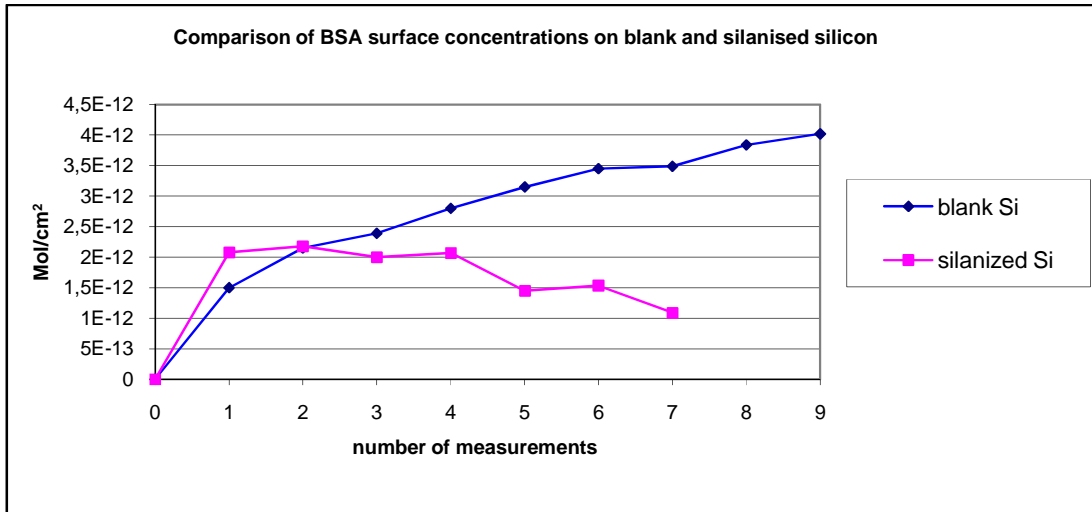


**Fig. 14.** Series of measurements at BSA concentrations of 25mg/ml with raising concentrations of NaCl (see Tab.1). At higher BSA concentrations unspecific adhesion to the surface or multiple layers of protein cannot be excluded.

**Tab. 1: Additional NaCl concentrations used in the experiments of Fig..**

Measurements #	blank Si	silanised Si
1	0 mM	0 mM
2	10 mM	10 mM
3	20 mM	20 mM
4	50 mM	50 mM
5	100 mM	100 mM
6	100 mM	200 mM
7	100 mM	200 mM
8	200 mM	
9	200 mM	

On silanised surfaces we achieved surface concentrations of BSA in the range of  $1,0 - 2,0 \text{ e-}12 \text{ Mol/cm}^2$ , whereas a monolayer of BSA in 100 mM NaCl yields surface concentrations of  $4,0 \text{ e-}12 \text{ Mol/cm}^2$  (Fig. 5, Tab. 1). The maximum surface concentration of BSA bound to an aldehyde layer was experimentally determined at  $2,2 \text{ e-}12 \text{ Mol/cm}^2$ . This means at a space of  $75 \text{ nm}^2$  one molecule of BSA is found. Compared to the  $33 \text{ nm}^2$  of a supposed monolayer this is quite scant. The silane obviously has an important effect on the surface concentration and acts as shielding against unspecific adhesion. This shielding effect is documented in the literature [46-48] and often used in other measurement techniques such as capillary electrophoresis [49]. Increased salt concentrations lead again to higher surface concentrations on blank silicon, but had no real effect on a silanised surface. This is

considered the result of the shielding properties of a thorough silane layer. The reduced surface concentration beginning with the 5<sup>th</sup> measurement is caused by equilibrium effects during the nighttime before the 6<sup>th</sup> measurement. Since the surface was not stored in a saturated BSA solution, some BSA detached from the surface and went into the bulk solution.

### **3.4 Surface concentration of covalently bound BSA on aldehyde silane surface**

The experimentally derived maximum value for a BSA-monolayer is  $5,0 \cdot 10^{-12}$  Mol/cm<sup>2</sup> [44]. The experimental conditions to reach that value involved using 200 mM NaCl in the buffer solution. NaCl is not used in the protocols of Patolsky et al. [11], because it interferes with the electrical charges on the surfaces of the nanowire, thus compromising its functionality. The chemical modification is the same imine reduction reaction described above in the materials and methods section.

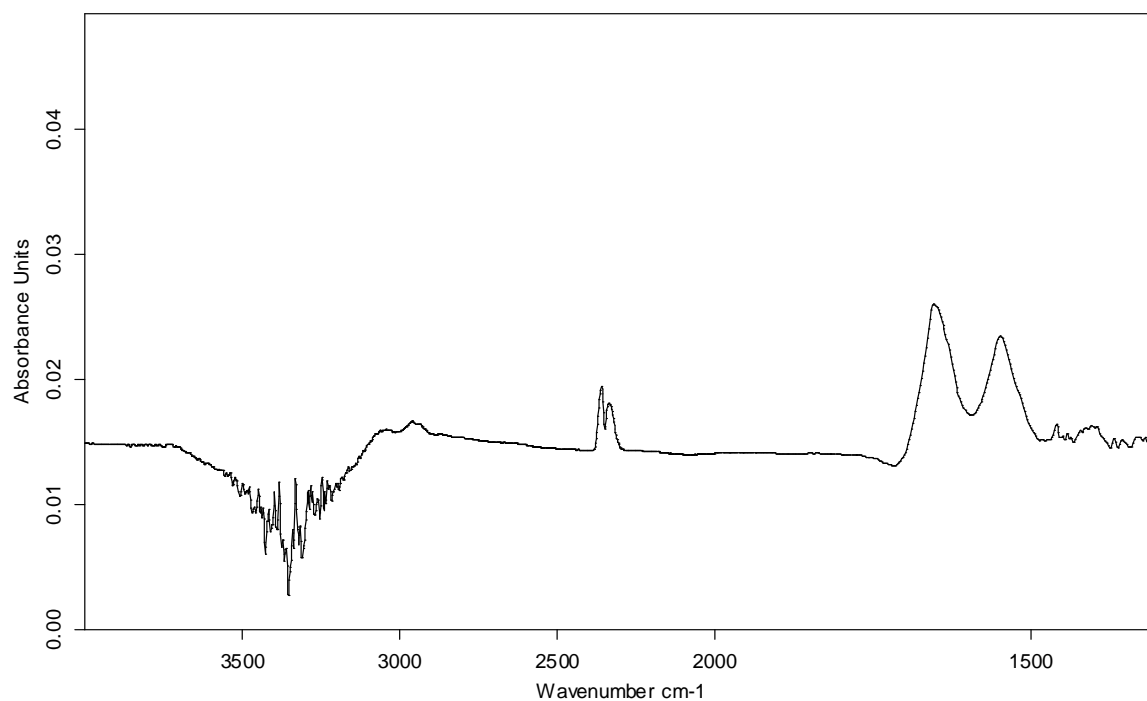


**Fig. 15. Absorbance spectrum of BSA on aldehyde silane (compressed wave number display). The amide I ( $1640\text{ cm}^{-1}$ ) and amide II ( $1540\text{ cm}^{-1}$ ) bands are clearly distinguishable. Only the amide II band is used for evaluation, because amide I can be overlapped by uncompensated water between reference and sample measurement. Other prominent bands are incompenations of the  $\text{H}_2\text{O}$  stretching vibration at  $3400\text{ cm}^{-1}$  and the  $\text{CO}_2$  stretching vibration at  $2400\text{ cm}^{-1}$ .**

### 3.5 Insulin on aldehyde-silane layer

Since BSA is known to unspecifically adhere to all kinds of surfaces, bovine insulin was used as another protein in further experiments. Preliminary experiments showed

that insulin also adheres to silicon, but much less than BSA. Insulin has low solubility in basic solutions, but since the necessary concentrations are very low (100  $\mu\text{g/ml}$ ) this did not cause any further problems. Experiments showed that no detectable amounts of insulin were unspecifically bound to the aldehyde surface after a wash with a 10% SDS solution (Fig. 6).

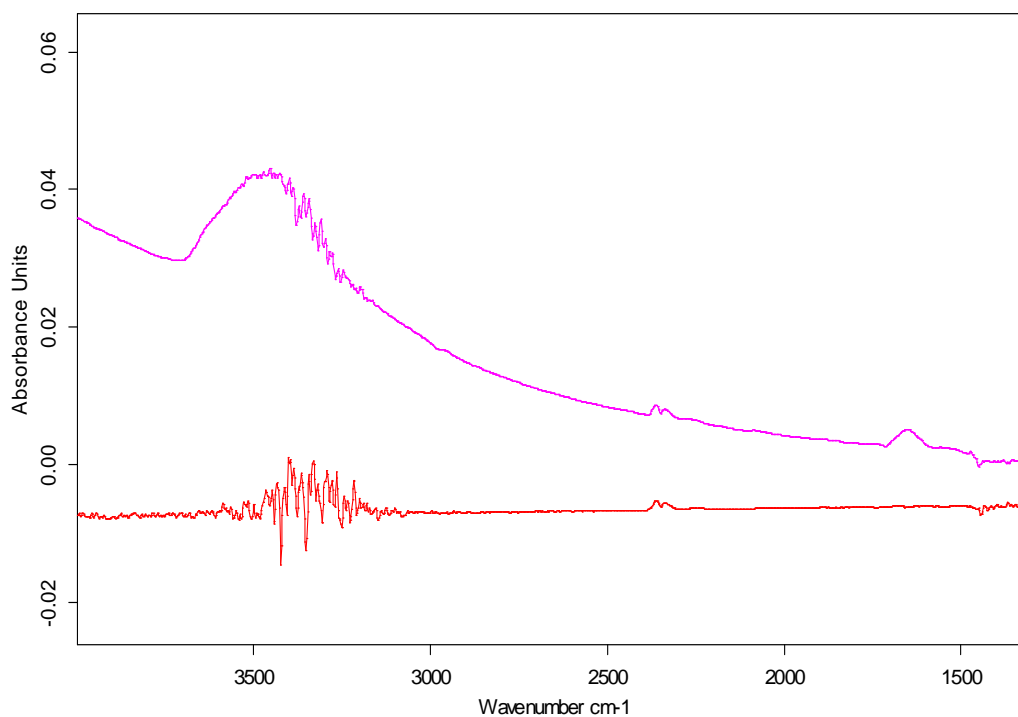


**Fig. 16. Spectrum 1 (magenta) shows bound insulin on an aldehyde surface. The amide I ( $1640\text{ cm}^{-1}$ ) band is combined with the bending vibration of water and thus not useable for quantification. The amide II ( $1540\text{ cm}^{-1}$ ) vibration is used to determine the surface concentration and exhibits a lower signal than amide I. Spectrum 2 (red) shows the protein layer after a wash with 10% SDS**

**solution. No further vibrational bands can be seen or evaluated, except the CO<sub>2</sub>-stretching vibration at 2300 cm<sup>-1</sup>.**

Insulin is bound to the silan layer with the same imine-reduction method described above in the methods section. The resulting surface concentrations for monomers vary between 1.2 e-12 Mol/cm<sup>2</sup> and 2.4 e-12 Mol/cm<sup>2</sup>. This corresponds to a surface requirement between 138 nm<sup>2</sup> and 66 nm<sup>2</sup> of one insuline molecule. The surface concentrations were one order of magnitude lower than the theoretical value of an insulin monolayer (2 e-11 Mol/cm<sup>2</sup>, Fig. 6). Despite the different size of BSA (MW = 66.000 kDa) and insuline monomer (MW = 5.800 kDa) the surface concentrations on an aldehyde surface are almost the same. Insuline can also exist as a hexamer with molecular weight of about 35.000 kDa especially at a pH of 7.4 to 8.4 [50]. For a hexamer the required area is given as 25 nm<sup>2</sup> [51]. The remaining difference may be contributed to different isoelectric points of 4.7 for BSA and 5.5 for insulin, which also influences the surface concentrations.

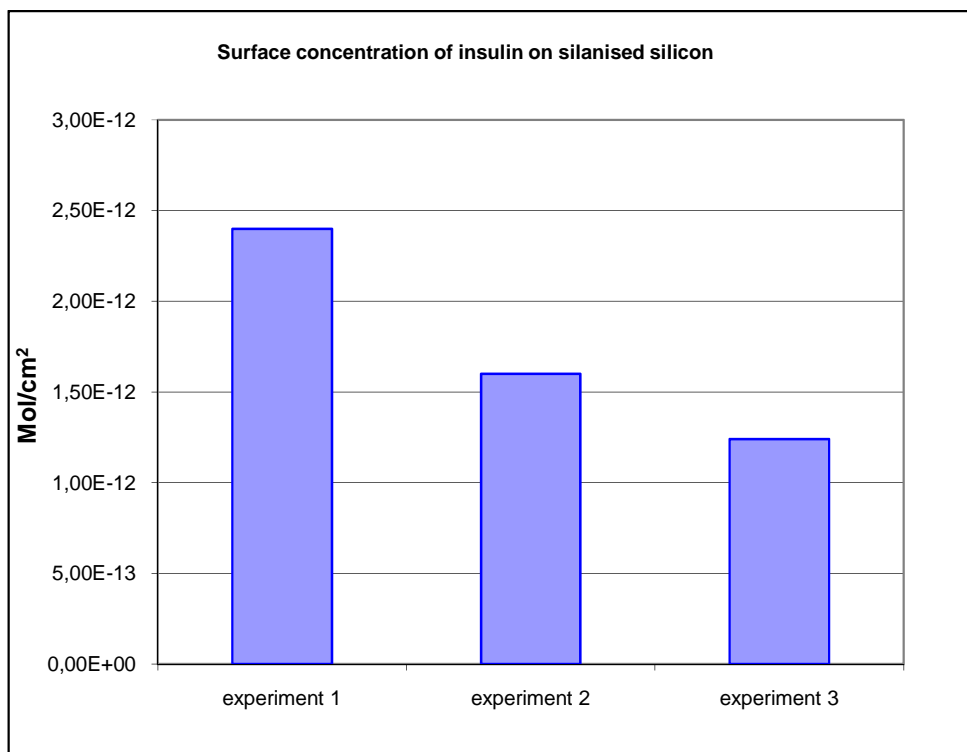


**Fig. 17. Insulin binding experiments on three silanised silicon surfaces. A protein concentration of 100 µg/ml was offered for 2h to the silanised silicon surfaces. Before measurement of the spectrum the protein solution was washed out and replaced by buffer. Resulting surface concentrations vary between 1,2 e-12 Mol/cm<sup>2</sup> and 2,4 e-12 Mol/cm<sup>2</sup>.**

### 3.6 Streptavidin-Biotin on aldehyde silane layer

The well characterized system of the bacterial protein streptavidin and its ligand biotin is also used in this work [52]. The bacterial protein streptavidin is covalently bound to the aldehyde surface using the same imine-reduction reaction described above in the materials and methods section. The aim of this experiment was to

determine if it is possible to detect both the receptor and the ligand on the surface and to measure their respective concentrations, despite the fact that biotin is a very small molecule yet exhibiting C=O bonds that usually give strong distinctive vibration signals.

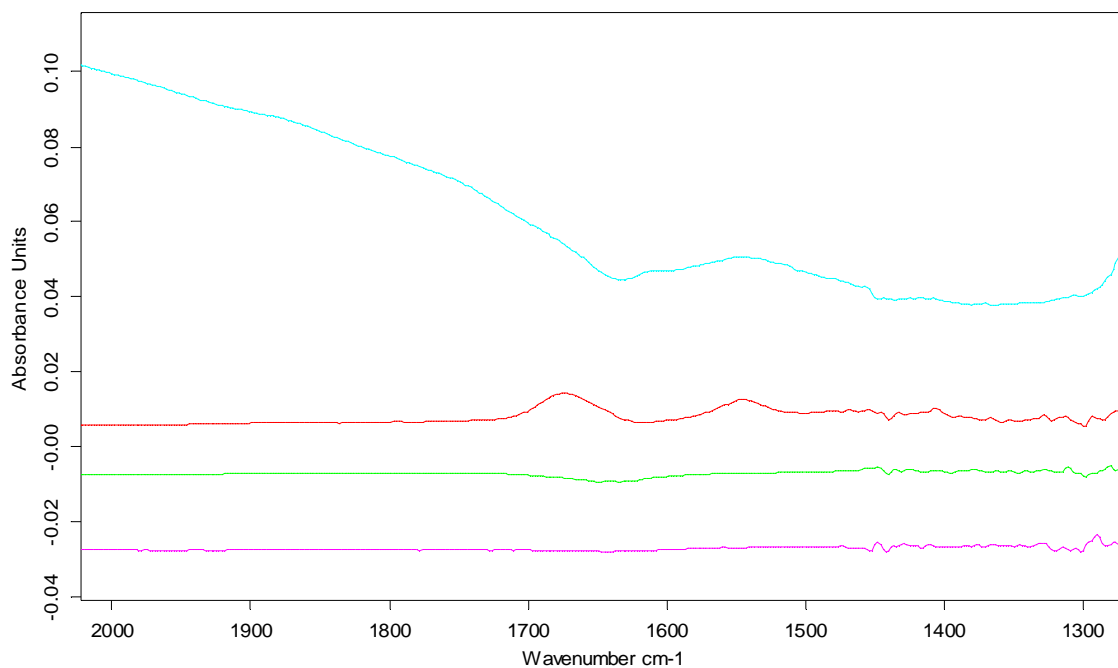
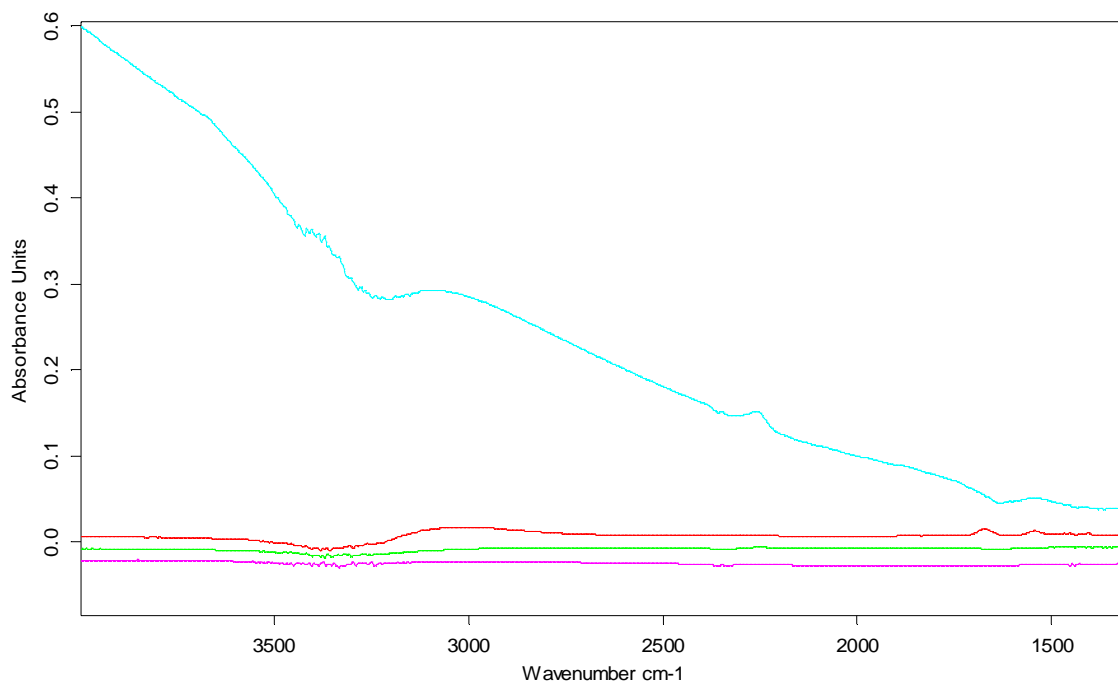
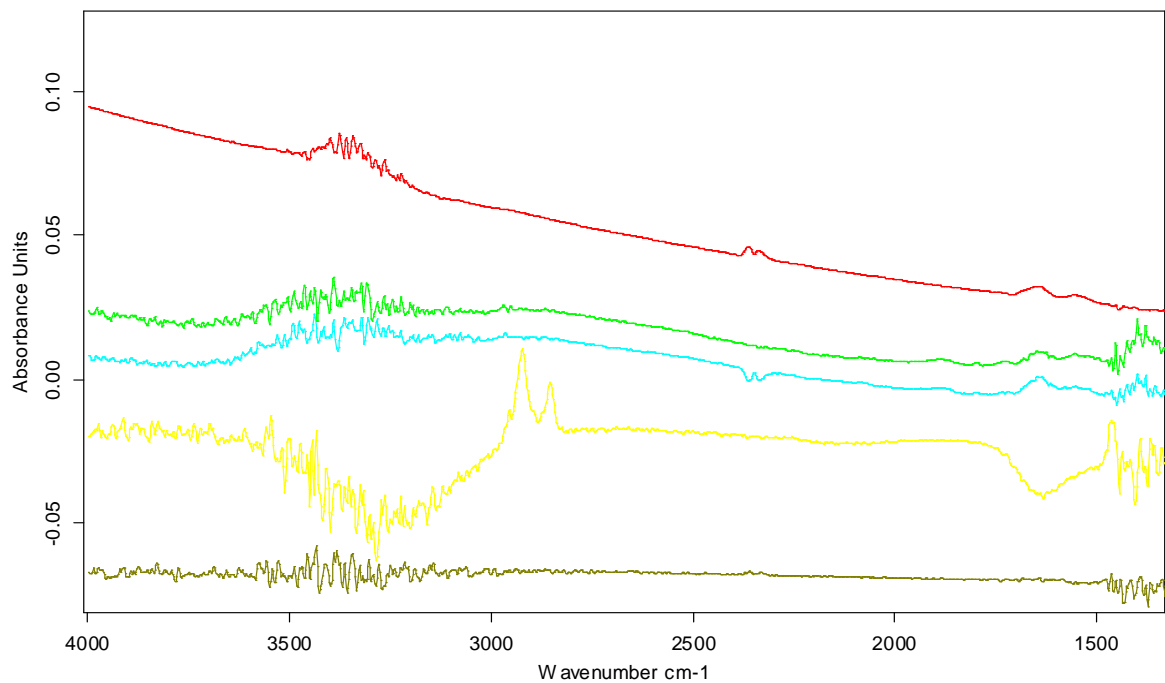


**Fig. 18 (A) and (B): Step by step spectra of streptavidin layer and supposedly attached biotin. Fig. B is a zoomed display of the relevant 1540 cm<sup>-1</sup> area. The first spectrum shows the streptavidin layer with the evaluated amide 2 vibration at 1540 cm<sup>-1</sup>. Second spectrum shows the biotin bulk solution with clear NH<sub>2</sub> vibrations at 1680 cm<sup>-1</sup> and 1550 cm<sup>-1</sup>. Third spectrum was recorded after a buffer wash to flush out any superfluous and unbound biotin. It does not show any vibrations except a H<sub>2</sub>O incompensation at 1640 cm<sup>-1</sup>. The fourth spectrum was measured after a thorough SDS-solution wash (10% SDS in buffer). It shows no negative amide vibrations, thus no protein is washed away from the surface.**

The surface concentration of streptavidin is evaluated at 1,25 e-12 Mol/cm<sup>2</sup>. This means every 140 nm<sup>2</sup> one molecule of streptavidin is attached to the surface. Nelson et al. [53] describe a two-dimensional streptavidin crystal with a surface concentration of 5,3 e-12 Mol/cm<sup>2</sup>, which means one molecule every 31 nm<sup>2</sup>. Again a fully covered monolayer could not be achieved. It is not possible to detect biotin attached to streptavidin. This is most likely, because the molecule is too small to be detected by FTIR-ATR in such a low surface concentration. It would be possible to do the experiment reversely. Biotin is attached to the surface and allows streptavidin to bind it on the surface. However the chemical mechanisms needed to be changed to accomplish this. Since this would stray too far from the original aim of this work it has not been done.

### 3.7 Surface concentrations of TNF- $\alpha$ anti-body on silanised silicon and captured TNF- $\alpha$ [34]

For reasons of cost efficiency a model system was used before advancing to the original prostate specific antigen protocol established by Patolsky et al. [11]. This model system involves TNF- $\alpha$  antibody and its antigen TNF- $\alpha$ . Since a biosensor should provide the possibility to detect actual antigens a concentration series for TNF- $\alpha$  ranging from 1  $\mu\text{g/ml}$  to 18  $\mu\text{g/ml}$  was tested on the antibody surface.



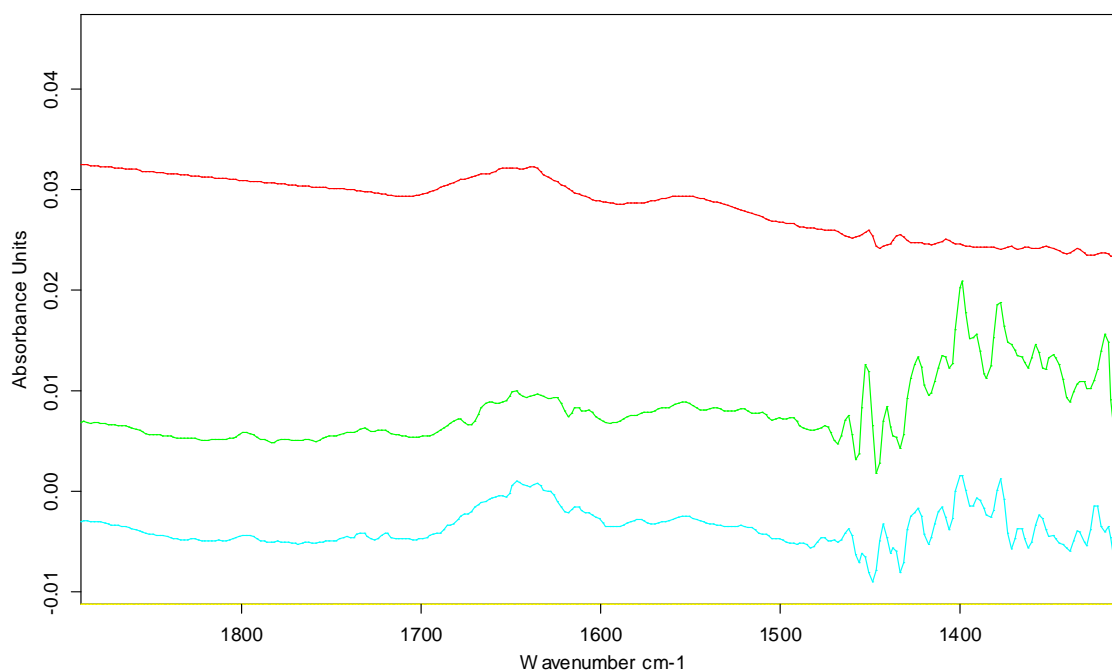


**Fig. 19 (A) and (B) (zoom display of amide 1 and 2 area): Absorbance spectra of step by step chemical modification of a silicon surface. Spectrum 1 shows the two amide bonds at  $1640\text{ cm}^{-1}$  (amide 1) and  $1540\text{ cm}^{-1}$  (amide 2) after TNF- $\alpha$  antibody attachment to the aldehyde layer. The baseline shift is caused by a change in optical properties of the system induced by the antibody. Spectrum 2 was taken with the antigen TNF- $\alpha$  bulk solution still in the s-compartment. It shows no relevant differences compared to spectrum 3, which represents the TNF- $\alpha$  layer after flushing out superfluous protein solution. The amide 1 and 2 vibrations are distinguishable. In spectrum 4 we see prominent bands of vibrations in the range of  $2850\text{ cm}^{-1}$  to  $2950\text{ cm}^{-1}$  corresponding to  $\text{CH}_2$  and  $\text{CH}_3$  vibrations of the SDS-bulk solution. At  $1640\text{ cm}^{-1}$  the bending vibration of water leads to considerable incompensation, caused by tiny air bubbles in the**

**system. Spectrum 5 represents the control experiment to evaluate the amount of washed out protein. It shows no visible amide 1 or 2 vibration meaning there was no protein washed away by the SDS-wash. In all spectra the H<sub>2</sub>O stretching vibration at 3400 cm<sup>-1</sup> is visible and causes a detector cut-off due to extreme absorbance. At 2400 cm<sup>-1</sup> there is the CO<sub>2</sub>-stretching vibration indicating an incompensation and starting at 1480 cm<sup>-1</sup> the silicon ATR-element cuts off the signal.**

Quantification of the amide 2 vibrations resulted in a surface concentration between 1,6 e-13 Mol/cm<sup>2</sup> and 1,7 e-13 mol/cm<sup>2</sup> for the anti-TNF- $\alpha$  antibody. This means one antibody molecule occupies a space of 1000 nm<sup>2</sup>. Surface concentrations for captured TNF- $\alpha$  antigen were between 0,9 e-13 mol/cm<sup>2</sup> and 3,9 e-13 mol/cm<sup>2</sup> (see Fig. 12). The antibody/antigen ratio was between 0,5 and 2,1.

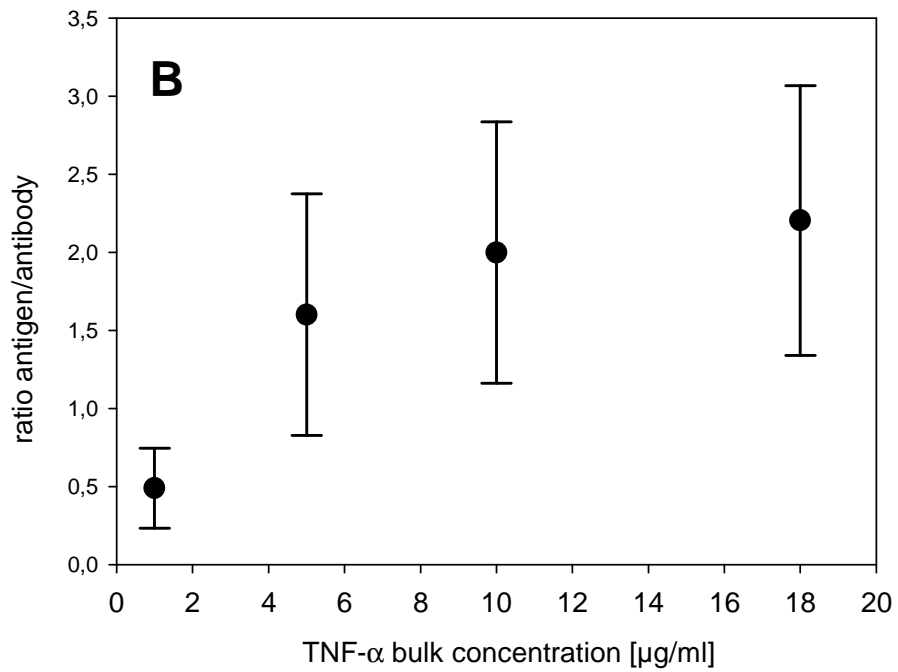
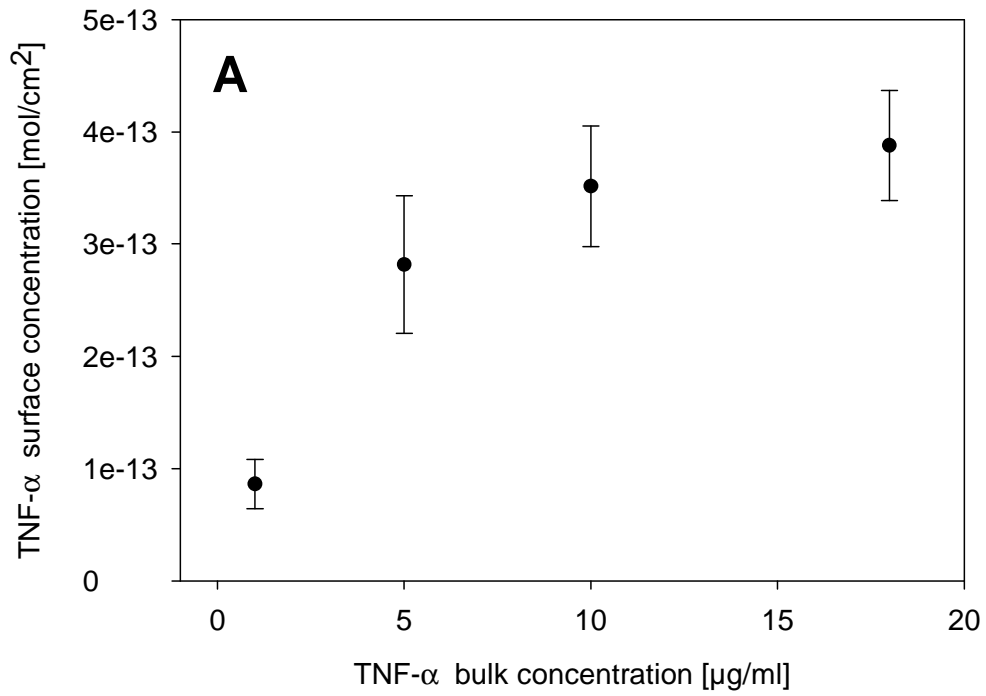
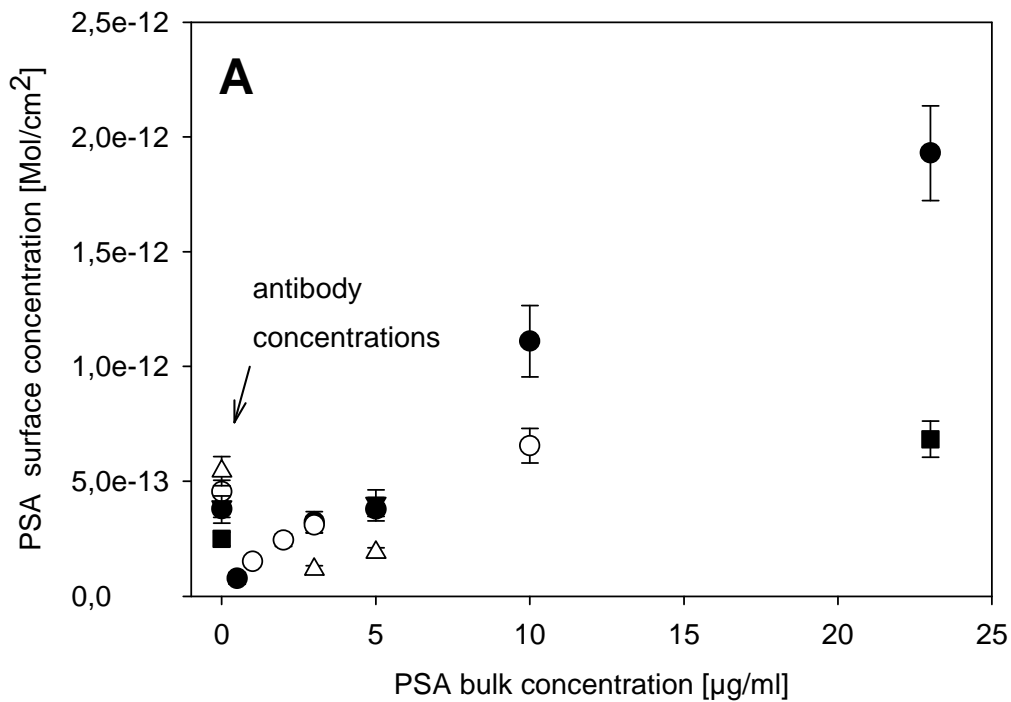


**Fig. 20 (A) and (B) [34]: Concentration series and binding test of TNF- $\alpha$  on anti-TNF- $\alpha$  antibody surface. The ratio between antibody and antigen exhibits an exponential curve with a maximum slightly higher than 2. Since one IgG antibody can bind 2 antigens the results are expected.**

The results of the TNF- $\alpha$  experiments show a maximum surface concentration of  $3,9 \text{ e-}13 \text{ mol/cm}^2$  for captured TNF- $\alpha$ . This is lower than measured in previous works by Hassler [44], who had a higher surface concentration of  $7,51 \text{ e-}12 \text{ mol/cm}^2$ . However Hassler did not bind the antibody on an aldehyde silane layer and then let the antibody surface capture the antigen. His approach was up-side down: with TNF- $\alpha$  adsorbed to the blank Germanium surface and an antibody solution afterwards like in an ELISA. The measured surface concentration translates into  $1000 \text{ nm}^2$  of used area per bound antibody molecule. Hasslers antibody/antigen ratio was 5,33, which is probably due to unspecific adhesion of binding of the antibody, despite a BSA passivation step. Since the antibody/antigen ratio in this work gave 2, the maximum possible for an IgG antibody, the whole linker/protein construct is considered working and functional. Bulk concentrations lower than  $1 \mu\text{g/ml}$  are not feasibly detected with the method in this work. Regarding detection limits in these experiments, the lowest absorption amplitude was  $50 \mu\text{AU}$  for parallel polarized IR-light. This corresponds to a peak integral of  $2,7 \text{ e-}13 \text{ cm-}1$  resulting in a detection limit of  $2,6 \text{ e-}14 \text{ mol cm-}1$ .

### 3.8 PSA-antibody and PSA on aldehyde surface [34]

These experiments were conducted to investigate the prototype biosensor using a PSA-antibody/PSA-antigen system established by Patolsky et al. [11] Mouse anti-PSA antibodies are bound to the aldehyde-surface and after passivation with ethanolamine another concentration series of PSA ranging from 5 ng/ml to 23  $\mu\text{g/ml}$  was pumped onto the antibody surface.



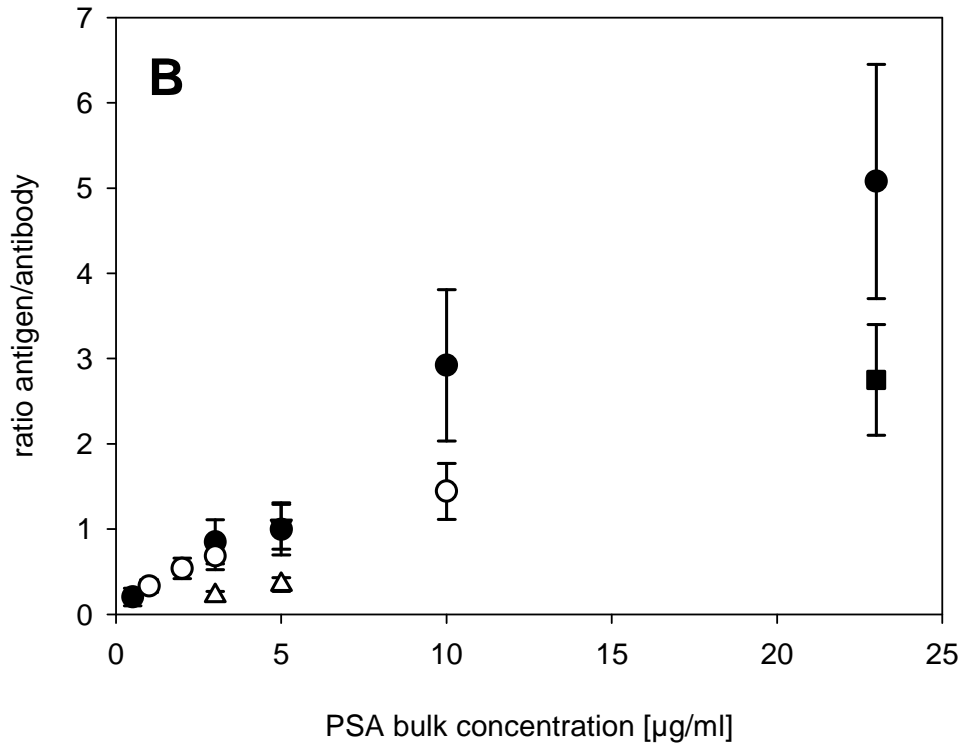


**Fig. 21 (A) and (B) [34]: Concentrations of anti-PSA antibody surface and PSA concentration series (combined view). The antibody concentrations are shown at zero PSA bulk concentration. Binding ratios in (B) correspond with the binding maximum of IgG antibodies, except for one experiment in which the ratio is clearly too high - possibly due to unspecific adhesion.**

The surface concentrations of anti-PSA antibody were determined between  $3,2 - 6,1 \cdot 10^{-13} \text{ mol/cm}^2$ . Captured PSA concentrations were between  $0,9 \cdot 10^{-13} \text{ mol/cm}^2$  and  $2,0 \cdot 10^{-12} \text{ mol/cm}^2$ . PSA solutions in the range of 5 ng/ml to 500 ng/ml showed no detectable signals. Neither in the bulk solution nor bound after a washing step. PSA solutions with more than 10 µg/ml showed an unexpected ratio between antibodies

and antigen. This could be due to unspecific adhesion. The surface concentrations of the anti-PSA antibody result in a used area between  $270 \text{ nm}^2$  and  $520 \text{ nm}^2$  for one antibody molecule. This corresponds quite well with the TNF- $\alpha$  results. According to literature the diameter of an IgG antibody is between 16 nm and 28 nm [54, 55]. Translated into square-cross sections this gives  $256 \text{ nm}^2$  to  $784 \text{ nm}^2$ . So the author assumes an almost closed monolayer of antibodies. The ratio of antibody to antigen was between 0,3 and 2,6. One experimental series showed a considerably higher ratio of 5. This is considered an aberration, most likely due to some unspecific adsorption. The detection limit for this experimental series was 100  $\mu\text{AU}$  for parallel polarized IR-light with a corresponding peak area of  $5,0 \text{ e-}3 \text{ cm}^{-1}$ . This leads to a detection limit of  $5,13 \text{ e-}14 \text{ mol cm}^{-2}$ .

### **3.9 Passivation of antibody surface with ethanolamine**

For this experimental step the symmetric  $\text{CH}_2$  vibration was used to determine the surface concentration. Measured surface concentrations of the passivation step were  $2,3 \text{ e-}10 \text{ Mol cm}^{-2}$  for one experiment. Actual results were very hard to achieve, because the basic buffer solution with a pH of 8.4 was either damaging the antibody surface or otherwise delivering inconclusive results. The end-capping with ethanolamine succeeded in only a couple of experiments, despite the fact that it was done in all experiments regarding antibodies and earlier protein experiments. The experimental procedure had to be changed to a reaction time of 30 min at maximum. Longer reaction times severely tempered with the protein surfaces and lead to the

removal of bound protein. The measured surface concentration of  $2,3 \text{ e-}10 \text{ Mol cm}^{-2}$  means that about one-third of the the aldehyde groups were capped with ethanolamine. Further adaptations of the original protocol or possibly other chemical mechanism are necessary to achieve more stable results.

### **3.10 DNA binding and corresponding sequence detection**

One of the main goals of biosensor functionality is the screening for certain RNA or DNA sequences. So a test system was tried with a DNA 20-mer probe-sequence and a complementary target-sequence.

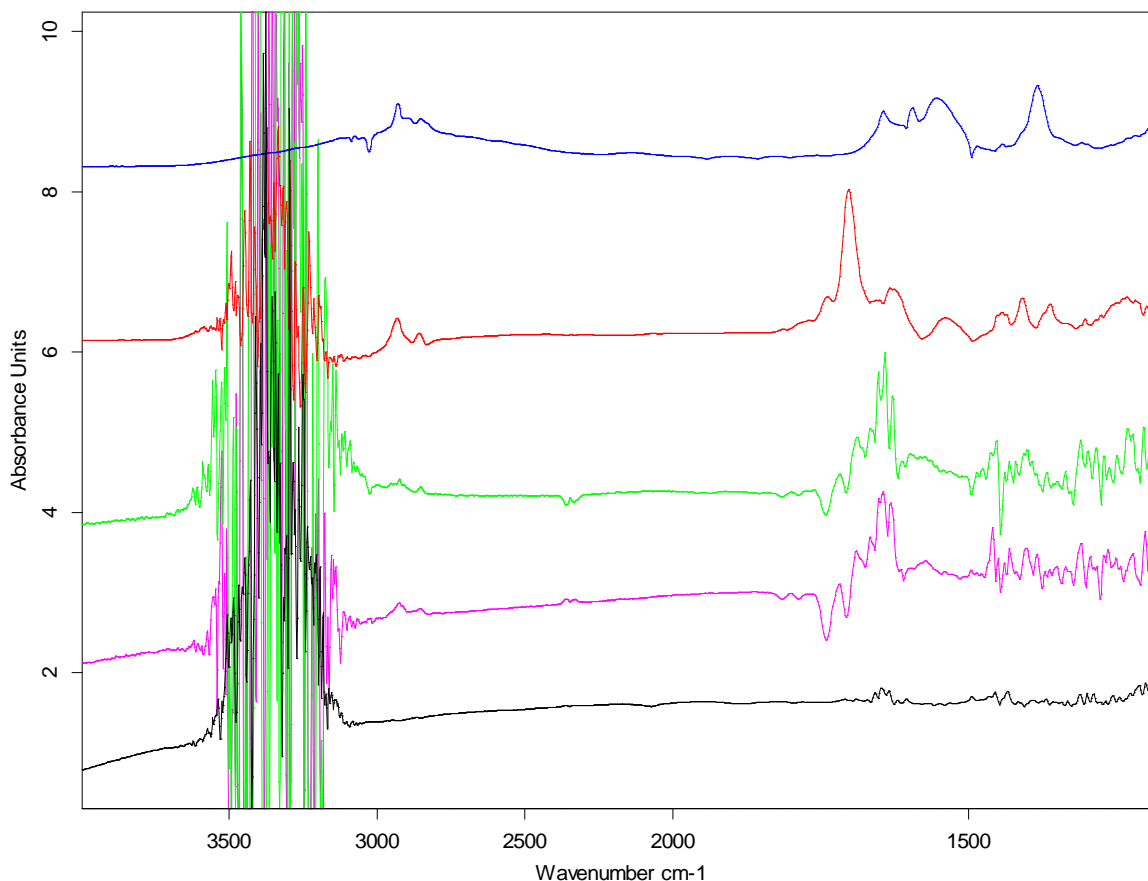


**Fig. 22. Step-by-step modification of silicon MIRE to resemble a DNA biosensor. Spectrum 1 (blue) shows the successful silanisation with APTES. The second spectrum (red) shows the bound SMCC cross-linker and its distinguished C=O vibration at 1700 cm<sup>-1</sup>. The third spectrum (green) shows bulk DNA and its complex vibration pattern from 1700 cm<sup>-1</sup> to 1500 cm<sup>-1</sup>. Spectrum 4 (magenta) shows putatively bound DNA after a buffer wash step. The last spectrum (black) shows target DNA on the sensor surface, however no useable signals are recognizable.**

The DNA experiments yielded no quantitatively evaluable data. This could be due to too harsh experimental conditions. DNA spectra showed negative peaks at 1740 cm<sup>-1</sup>

<sup>1</sup> and 1700 cm<sup>-1</sup>, which hint to the detachment of the SMCC cross-linker. Further adaptations of the original protocol to our test system could not be made, because of time limitations.

**Table 2: Surface concentrations of proteins bound on silanised surfaces and antigens bound to corresponding antibodies.**

protein	concentration of protein bulk solution [µg/ml]	measured surface concentration [mol/cm <sup>2</sup> ]	corresponding area per molecule [nm <sup>2</sup> ]	required area per molecule from literature [nm <sup>2</sup> ]	molecular weight [kDa]
insuline	100	1.2 e-12 - 2.4 e-12	140 - 69	4 (single molecule) [51]	5.8
				25 (hexamer) [51]	
BSA	100	1.5 e-12 - 2.4 e-12	110 - 33	56 [56]	67
anti-TNF-a	100	1.6 e-13 - 1.7 e-13	1100 - 970	784 [55]	146
				256 - 361 [54]	
TNF-a	5 - 18	1.7 e-13 - 2.73 e-13	ratio: TNF-a/anti-TNF-a 1.0 - 1.6		17
anti-PSA	50	3.2 e-13 - 6.1 e-13	520 - 270	784 [55]	150
				256 - 361 [54]	
PSA	1 - 10	1.6 e-13 - 7 e-13	ratio: PSA/anti-PSA 0.3 - 1.4		34

#### 4 References

1. Ferguson, J.A., F.J. Steemers, and D.R. Walt, *High-Density Fiber-Optic DNA Random Microsphere Array*. Anal. Chem., 2000. **72**: p. 5618-5624.
2. Carrascosa, L.G., et al., *Nanomechanical biosensors: a new sensing tool*. Trends in Analytical Chemistry, 2005. **25**(3): p. 196-206.
3. Dutta, P., et al., *Development of a nanomechanical biosensor for analysis of endocrine disrupting chemicals*. Lab on a Chip, 2007. **7**(9): p. 1184-1191.
4. Lechuga, L.M., et al., *A highly sensitive microsystem based on nanomechanical biosensors for genomics applications*. Sensors and Actuators B: Chemical, 2006. **118**(1-2): p. 2-10.
5. Lee, J.H., et al., *Immunoassay of prostate-specific antigen (PSA) using resonant frequency shift of piezoelectric nanomechanical microcantilever*. Biosensors and Bioelectronics, 2005. **20**(10): p. 2157-2162.
6. Wang, X., et al., *Piezoelectric Field Effect Transistor and Nanoforce Sensor Based on a Single ZnO Nanowire*. Nano Letters, 2006. **6**(12): p. 2768-2772.
7. Benesa, E., et al., *Sensors based on piezoelectric resonators* Sensors and Actuators A: Physical, 1995. **48**(1): p. 1-21.
8. Dzyadevych, S.V., et al., *Enzyme biosensors based on ion-selective field-effect transistors*. Analytica Chimica Acta, 2006. **568**: p. 248-258.
9. Bergveld, P., *Development, Operation, and Application of the Ion-Sensitive Field-Effect Transistor as a Tool for Electrophysiology*. Biomedical Engineering, IEEE Transactions on, 1972. **BME-19**(5): p. 342-351.
10. Poghosian, A., J.W. Schultze, and M.J. Schöning, *Application of a (bio-)chemical sensor (ISFET) for the detection of physical parameters in liquids*. Electrochimica Acta, 2003. **48**(20-22): p. 3289-3297.
11. Patolsky, F., G. Zheng, and C.M. Lieber, *Fabrication of silicon nanowire devices for ultrasensitive, label-free, real-time detection of biological and chemical species*. Nat Protoc, 2006. **1**(4): p. 1711-1724.
12. Hsiao, C.Y., et al., *Novel poly-silicon nanowire field effect transistor for biosensing application*. Biosensors and Bioelectronics, 2009. **24**: p. 1223-1229.
13. Backmann, N., et al., *A label-free immunosensor array using single-chain antibody fragments*. PNAS, 2005. **102**(41): p. 14587-14592.
14. Stern, E., et al., *Label-free biomarker detection from whole blood*. Nature Nanotechnology, 2010. **5**: p. 138-142.
15. Wilchek, M., E.A. Bayer, and O. Livnah, *Essentials of biorecognition: The (strept)avidin-biotin system as a model for protein-protein and protein-ligand interaction*. Immunology Letters, 2006. **103**(1): p. 27-32.
16. Zheng, G., et al., *Multiplexed electrical detection of cancer markers with nanowire sensor array*. Nature Biotechnology, 2005. **23**(10): p. 1294-1301.
17. Sheenan, P.E. and L.J. Whitman, *Detection limits for nanoscale biosensors*. Nano Letters, 2005. **5**(4): p. 803-807.
18. Hunt, H. and A. Armani, *Label-free biological and chemical sensors*. Nanoscale, 2010. **2**: p. 1544-1559.

19. Hahm, J.I. and C.M. Lieber, *Direct Ultrasensitive Electron Detection of DNA and DNA Sequence Variations Using Nanowire Nanosensors*. Nano Letters, 2004. **4**(1): p. 41-54.
20. Baumgartner, S. and C. Heitzinger, *Existence and local uniqueness for 3d self-consistent multiscale models for field-effect sensors*. Commun. Math. Sci., 2012. **10**(2): p. 693–716.
21. Baumgartner, S., et al., *Optimization of nanowire DNA sensor sensitivity using self-consistent simulation*. Nanotechnology, 2011. **22**(425503)(42): p. 1-8.
22. Baumgartner, S., M. Vasicek, and C. Heitzinger, *Analysis of field-effect biosensors using self-consistent 3D drift-diffusion and Monte-Carlo simulations*. Procedia Engineering, 2011. **25**: p. 407-410.
23. Bulyha, A. and C. Heitzinger, *An algorithm for three-dimensional Monte-Carlo simulation of charge distribution at biofunctionalized surfaces*. Nanoscale, 2011. **3**: p. 1608-1617.
24. Heitzinger, C., et al., *Calculation of fluctuations in boundary layers of nanowire field-effect biosensors*. J. Comput. Theor. Nanosci., 2010. **7**(12): p. 2574–2580.
25. Heitzinger, C., N. Mauser, and C. Ringhofer, *Multiscale modeling of planar and nanowire field-effect biosensors*. SIAM J. Appl. Math., 2010. **70**(5): p. 1634–1654.
26. Goos, F.H., H., *Ein neuer und fundamentaler Versuch zur Totalreflexion* Annalen der Physik, 1947. **436**(7-8): p. 13.
27. Harrick, N.J., *Internal Reflection Spectroscopy*. 1979, Ossining (New York): Harrick Sci. Corp.
28. Fringeli, U.P., et al., *ATR spectroscopy of thin films*, in *Handbook of Thin Film Materials*, H.S. Nalwa, Editor. 2002, Academic Press: San Diego (USA). p. 191-229.
29. Peters, T., *Serum Albumin*. Adv. Protein Chem., 1985. **37**: p. 161-245.
30. Barbosa, L.R.S., et al., *The Importance of Protein-Protein Interactions on the pH-Induced Conformational Changes of Bovine Serum Albumin: A Small-Angle X-Ray Scattering Study*. Biophysical Journal, 2010. **98**: p. 147-157.
31. Fitzpatrick, H., et al., *Bovine serum albumin adsorption to mica surfaces*. Colloids and Surfaces, 1992. **65**: p. 43-49.
32. [www.chemgapedia.de](http://www.chemgapedia.de), *Ribbon model of tumor necrosis factor alpha*. 2014.
33. [www.dbc-labs.com](http://www.dbc-labs.com), *Ribbon model of prostate specific antigen*.
34. Punzet, M., et al., *Determination of surface concentrations of individual molecule-layers used in nanoscale biosensors by in situ ATR-FTIR spectroscopy*. Nanoscale, 2012. **4**(7): p. 2431-2438.
35. Hassler, N., et al., *In Situ FTIR ATR Spectroscopic Study of the Interaction of Immobilized Human Serum Albumin with Cholate in Aqueous Environment*. J. Phys. Chem. C, 2011. **115**: p. 1064–1072.
36. Fringeli, U.P., *In situ infrared attenuated total reflection membrane spectroscopy*, in *Internal Reflection Spectroscopy*, F.M. Mirabella Jr., Editor. 1992, CRC Press: New York. p. 255-324.
37. Baurecht, D., et al., *Application of Special FTIR-ATR Techniques for Quantitative Structural Analysis of Thin Surface Layers*. Chimia, 2005. **59**: p. 226-235.
38. Helmut Günzler, H.-U.G., *IR-Spektroskopie*. 2000, Weinheim: Wiley-VCH. 268.
39. Strother, T., R.J. Hamers, and L.M. Smith, *Covalent attachment of oligodeoxyribonucleotids to amine-modified Si (001) surfaces*. Nucleic Acids Research, 2000. **28**(18): p. 3535-3541.

40. Streifer, J.A., et al., *Covalent functionalization and biomolecular recognition properties of DNA-modified silicon nanowires*. Nanotechnology, 2005. **16**: p. 1868-1873.
41. Matijasevic, J., et al., *In Situ ATR FTIR Monitoring of the Formation of Functionalized Mono- and Multilayers on Germanium Substrate: from 7-Octenyltrichlorosilane to 7-Carboxylsilane*. Langmuir, 2008. **24**(6): p. 2588-2596.
42. Matijasevic, J., *Synthesis of biomimetic surfaces under permanent in situ FTIR ATR monitoring*, in *Institute of Biophysical Chemistry*. 2008, University of Vienna: Vienna. p. 134.
43. Melnikov, M.S., et al., *Influence of Residual Silanol Groups on Solvent and Ion Distribution at a Chemically Modified Silica Surface*. J. Phys. Chem. C, 2009. **113**: p. 9230-9238.
44. Hassler, N., *Interaction of tumor necrosis factor-alpha with an antibody and of albumin with cholate investigated by FTIR attenuated total reflection spectroscopy*, in *Institute of Biophysical Chemistry*. 2008, University of Vienna: Vienna.
45. Luey, J.K., J. McGuire, and R.D. Sproull, *The Effect of pH and NaCl Concentration on Adsorption of  $\beta$ -Lactoglobulin at Hydrophilic and Hydrophobic Silicon Surfaces*. Journal of Colloid and Interface Science, 1991. **143**(2): p. 489-500.
46. Sheila Mohabbati, S.H., Douglas Westerlund, *Influence of ignored and well-known zone distortions on the separation performance of proteins in capillary free zone electrophoresis with special reference to analysis in polyacrylamide-coated fused silica capillaries in various buffers*. Journal of Chromatography A, 2004. **1053**: p. 201-216.
47. H. Engelhardt, M.A.C.-W., *Preparation and stability tests for polyacrylamide-coated for capillary electrophoresis*. Journal of Chromatography A, 1995. **716**: p. 27-33.
48. Cretich, M., et al., *Electroosmotic flow suppression in capillary electrophoresis: chemisorption of trimethoxy silane-modified polydimethylacrylamide*. Electrophoresis, 2005. **26**(10): p. 1913-1919.
49. Margrét Thorsteinsdóttir and D.W. Roland Isaksson, *Performance of amino-silylated fused-silica capillaries for the separation of enkephalin-related peptides by capillary zone electrophoresis and micellar electrokinetic chromatography*. Electrophoresis, 1995. **16**(1): p. 557-563.
50. Nielsen, L., et al., *Probing the Mechanism of Insulin Fibril Formation with Insulin Mutants*. Biochemistry, 2001. **40**: p. 8397-8409.
51. Sakabe, N.S., K.; Sasaki, K., *X-ray studies of water structure in 2 Zn insulin crystal*. Proc. Int. Symp. Biomol. Struct. Interactions, Suppl. J. Biosci., 1985. **8**: p. 45-55.
52. Piscevic, D., W. Knoll, and M.J. Tarlov, *Surface plasmon microscopy of biotin-streptavidin binding reactions on UV-photopatterned alkanethiol self-assembled monolayers*. Supramolecular Science, 1995. **2**: p. 99-106.
53. Kjell, E.N., et al., *Surface Characterization of Mixed Self-Assembled Monolayers Designed for Streptavidin Immobilization*. Langmuir, 2001. **17**: p. 2807-2816.
54. Brady, R.L., et al., *Crystallization and preliminary X-ray diffraction study of a chimaeric Fab' fragment of antibody binding tumour cells*. J.Mol.Biol., 1991. **219**: p. 603.
55. Roberts, C.J., et al., *Real-space differentiation of IgG and IgM antibodies deposited on microtiter wells by scanning force microscopy*. Langmuir, 1995. **11**(5): p. 1822-1826.

56. Reiter, G., et al., *In situ FTIR ATR spectroscopic study of the interaction of immobilized human tumor necrosis factor- $\alpha$  with a monoclonal antibody in aqueous environment*. *Biochimica et Biophysica Acta*, 2004. **1699**: p. 253–261.

Hinweis:

Ich habe mich bemüht, sämtliche Inhaber der Bildrechte ausfindig zu machen und ihre Zustimmung zur Verwendung der Bilder in dieser Arbeit eingeholt. Sollte dennoch eine Urheberrechtsverletzung bekannt werden, ersuche ich um Meldung bei mir.

## Curriculum vitae

### Ausbildung

- 1998 Abgeschlossene Lehrausbildung als Elektromechaniker für Schwachstrom
- 2000 Matura am Abendgymnasium Linz
- 2000 – 2006 Studium der Genetik und molekularen Biologie an der Universität Salzburg  
Schwerpunkte: Immunologie, analytische Chemie, Proteinchemie  
Abschluss mit ausgezeichnetem Erfolg
- 2009 – 2012 Dissertation Infrarotspektroskopie, Universität Wien, Abschluss 2014
- 2/2004 – 3/2004 Arbeitsgruppe Prof. Ferreira, Universität Salzburg:  
Clonierung und Expression von Pflanzenallergenen,  
Proteinreinigung
- 4/2004 – 5/2004 Arbeitsgruppe Prof. Duschl, Universität Salzburg:  
Div. PCR Methoden, Gelelektrophorese, Umgang mit  
Versuchstieren (Mäuse), Genotypisierung von Mäusen
- 6/2004 Praktikum am Institut für Gerichtsmedizin in Salzburg:  
Vaterschaftstests, Erstellung von genetischen  
Fingerabdrücken
- 8/2004 Praktikum im Krankenhaus der Elisabethinen, Linz:  
PCR, RT-PCR, Untersuchung von Blutproben auf diverse  
Viren, Durchführung von DNA-Extraktionen
- 6/2005 - 7/2005 Tutor, Universität Salzburg:  
Abhalten von Kursen für allgemeine Chemie, sowie  
analytische Chemie (HPLC)
- 9/2004 – 7/2005 Diplomarbeit, Arbeitsgruppe Prof. Malissa, Universität Salzburg:  
Proteinanalyse mittels Kapillarelektrophorese (CZE,  
cIEF), Peptide mapping mittels Massenspektrometrie
- Publikation: "Profiling preparations of recombinant birch pollen allergen Bet v 1a with capillary zone

electrophoresis in pentamine modified fused-silica capillaries” im Journal of Chromatography B (2006).

- 10/2006 – 8/2007 Dissertation, Arbeitsgruppe Prof. Hinterdorfer, Universität Linz:  
Atomkraftmikroskopiestudien an nativen Xenopus-Oocytenzellkernen, Messung von Protein-Protein Interaktionen (Kraftspektroskopie), Kapillarelektrophorese, native Gelelektrophorese, Oberflächenchemie, Umgang mit Versuchstieren (*Xenopus laevis*)
- 2/2009 – 1/2012 Dissertation, Arbeitsgruppe Prof. Rempel, Universität Wien  
Infrarotspektroskopie, Oberflächenchemie (org. und biolog. Moleküle)
- Publikation: Determination of surface concentrations of individual molecule-layers used in nanoscale biosensors by in situ ATR-FTIR spectroscopy (Nanoscale 2012)

## Determination of surface concentrations of individual molecule-layers used in nanoscale biosensors by *in situ* ATR-FTIR spectroscopy

Manuel Punzet,<sup>a</sup> Dieter Baurecht,<sup>\*a</sup> Franz Varga,<sup>b</sup> Heidrun Karlic<sup>c</sup> and Clemens Heitzinger<sup>de</sup>

Received 20th December 2011, Accepted 2nd February 2012

DOI: 10.1039/c2nr12038k

For the development of nanowire sensors for chemical and medical detection purposes, the optimal functionalization of the surface is a mandatory component. Quantitative ATR-FTIR spectroscopy was used *in situ* to investigate the step-by-step layer formation of typical functionalization protocols and to determine the respective molecule surface concentrations. BSA, anti-TNF- $\alpha$  and anti-PSA antibodies were bound *via* 3-(trimethoxy)butylsilyl aldehyde linkers to silicon-oxide surfaces in order to investigate surface functionalization of nanowires. Maximum determined surface concentrations were  $7.17 \times 10^{-13}$  mol cm<sup>-2</sup> for BSA,  $1.7 \times 10^{-13}$  mol cm<sup>-2</sup> for anti-TNF- $\alpha$  antibody,  $6.1 \times 10^{-13}$  mol cm<sup>-2</sup> for anti-PSA antibody,  $3.88 \times 10^{-13}$  mol cm<sup>-2</sup> for TNF- $\alpha$  and  $7.0 \times 10^{-13}$  mol cm<sup>-2</sup> for PSA. Furthermore we performed antibody–antigen binding experiments and determined the specific binding ratios. The maximum possible ratio of 2 was obtained at bulk concentrations of the antigen in the  $\mu\text{g ml}^{-1}$  range for TNF- $\alpha$  and PSA.

### Introduction

Development of nanoscale sensor devices for the label-free detection<sup>1–4</sup> of DNA and various biological markers plays an important role in future medical diagnostic systems. Current devices work *via* piezoelectric effects,<sup>5,6</sup> in combination with field effects,<sup>7</sup> *via* nanomechanical effects<sup>8–11</sup> or as semi-conductor field-effect transistors (FET).<sup>2,12,13</sup> Fields of application involve structural monitoring and sensing of biological molecules and chemical compounds such as the detection of cancer markers in blood analysis.<sup>2,14</sup> In the case of field-effect nanowire sensors, the binding of target molecules changes the charge concentration at the surface; this effect acts like a gate contact and modulates the current through the transducer. Advantages of this technique are the direct conversion of a chemical or biochemical signal to an electrical signal without any intermediates like fluorescent markers or optical systems, *i.e.* a label-free detection is achieved. The sensitivity of nanowire sensors is unparalleled with detection limits for DNA in the femtomolar range,<sup>12,15</sup> and proteins can be detected in the picomolar range.<sup>16</sup>

Although methods for surface functionalization are known,<sup>14,17,18</sup> the density of the functionalized layer depends on many process parameters of the single steps of surface functionalization including the attachment of linkers. Without the ability to check the quality of the single steps of surface functionalization, it is very time consuming to determine the influence of the various process parameters. Therefore *in situ* FTIR measurements were used in this work to characterize the step-by-step formation of the functionalized surface.

FTIR spectroscopy is well known to be able to characterize chemical modifications of surfaces by the use of attenuated total reflection (ATR),<sup>19–32</sup> infrared reflection–absorption spectroscopy (IRRAS)<sup>33</sup> or grazing-angle attenuated total reflection (GATR).<sup>18</sup> The former is also able to quantitatively determine surface concentrations.<sup>34,35</sup> As FTIR-ATR techniques directly measure chemical information of the molecules, we can quantify molecule concentrations on the chemical basis of functional groups of the unmodified molecules. This is a considerable advantage compared to techniques that need molecular labeling (*e.g.* fluorescence measurements), techniques that are only able to measure the changes of masses (*e.g.* quartz crystal microbalance measurements) or techniques that use relatively unspecific changes of the refractive indices without the information from which molecules these changes result from (*e.g.* surface plasmon resonance measurements).

In this work, we determined surface concentrations of proteins attached to silicon-oxide surfaces by FTIR-ATR spectroscopy. Moreover, we determined resulting antibody–antigen ratios for two different systems. The fact that silicon is not only used as the semiconducting transducer, but also serves as an internal-reflection element in FTIR-ATR-spectroscopy, offers the ability

<sup>a</sup>Institute of Biophysical Chemistry, University of Vienna, Althanstraße 14, A-1090 Vienna, Austria. E-mail: dieter.baurecht@univie.ac.at

<sup>b</sup>Ludwig Boltzmann Institute of Osteology, Hanusch Hospital, Heinrich Collin-Straße 30, A-1140 Vienna, Austria

<sup>c</sup>Ludwig Boltzmann Institute for Leukemia Research and Cluster Oncology, Hanusch Hospital, Heinrich Collin-Straße 30, A-1140 Vienna, Austria

<sup>d</sup>Department of Mathematics, University of Vienna, Nordbergstrasse 15, A-1090 Vienna, Austria

<sup>e</sup>Department of Applied Mathematics and Theoretical Physics (DAMTP), University of Cambridge, Cambridge CB3 0WA, UK

to investigate silicon-oxide surfaces by FTIR-spectroscopy. We also demonstrate how to use FTIR-ATR spectroscopy as a tool for the determination of surface concentrations of monomolecular layers and chemical binding properties of surface modifications utilized in nanowire sensors. This method can be used to optimize surface-modification protocols, which are essential for the development of nanowire sensors.

The resulting data are also used in numerical simulations in order to provide the quantitative understanding of the sensing mechanism of field-effect sensors. To this end, a self-consistent partial-differential-equations model<sup>36–38</sup> was developed as well as a Metropolis-Monte-Carlo algorithm<sup>39</sup> for the quantification of screening by free ions. Other screening models have been developed as well.<sup>40,41</sup> Using our simulations, we can determine optimal device parameters and the optimal operating regime.<sup>42–44</sup>

## Experimental

### Chemicals

Bovine serum albumin (BSA) was bought from Sigma-Aldrich (Buchs, Switzerland). 3-(Trimethoxy)butylsilyl aldehyde was purchased from United Chemical Technologies, Inc. (Bristol, PA, USA). Prostate-specific antigen-antibody was purchased from Fisher Scientific and Prostate specific antigen (PSA) from Calbiochem (La Jolla, CA, USA). Human tumor necrosis factor- $\alpha$  (TNF- $\alpha$ ) was purchased from Stratham Biotec AG. Monoclonal hTNF- $\alpha$  antibody was obtained from the Center for Biomedical Technology (Danube University, Krems, Austria). Sodium cyanoborohydride and ethanolamine were bought from Sigma-Aldrich (Steinheim, Germany). PTFE syringe filters with 20  $\mu\text{m}$  cut-off were purchased from Sartorius (Germany). 10 mM potassium and sodium phosphate buffer at pH 8.4 was used as the buffer during the binding of all proteins to the silane surface. For the antigen capture experiments 10 mM potassium phosphate and 10 mM sodium phosphate at pH 7.4 with additional 2  $\mu\text{M}$  KCl was used as the buffer solution. 96% ethanol was prepared with spectroscopic grade absolute ethanol and ultra pure water. All aqueous solutions were prepared using ultra pure water and degassed prior to use.

### FTIR measurements

All FTIR-ATR spectra were measured at 25 °C with a Bruker IFS 66 FTIR spectrometer using a MCT detector. Trapezoidal shaped multiple internal reflection elements (MIREs, base length 52 mm, width 20 mm and thickness 1.5 mm) made of silicon were used as ATR-elements. The surface was chemically polished with a polishing machine (Logitech PM-5) using amorphous silica suspension (Logitech SF-1) on a polyurethane polishing cloth (Logitech). After polishing and cleaning, the element was refluxed for 4 h in 70% nitric acid to activate the silicon surface by oxidation and remove any metal ions interfering with the silanization reaction later. The final preparation step was a 3 min plasma cleaning (Harrick Plasma cleaner). For polarization of the incident IR-beam an aluminium grid polarizer on a KRS-5 substrate (Specac, Orpington, UK) was used. The ATR angle of incidence  $\theta$  was set at 45°. FTIR spectra were recorded at 4  $\text{cm}^{-1}$  resolution using Blackham-

Harris 3-term apodization and a zero filling factor of 4. Interferograms were measured in double sided mode that needs no phase correction, due to small sample absorbances in a high background absorbance, *e.g.* H<sub>2</sub>O of buffer. Thermostatted flow-through cells made of Delrin® were used to mount the MIREs and to simultaneously surround the measurement compartments. To determine molar absorbance coefficients, transmission spectra were recorded using a Bruker IFS 25 with a DTGS detector at 4  $\text{cm}^{-1}$  resolution using single-sided mode and Mertz phase correction. The transmission cell consisted of calcium fluoride windows and Mylar® spacers with a determined real thickness of 24.7  $\mu\text{m}$ .<sup>45</sup> Spectrometers were constantly purged with dry, carbon dioxide free air and set up on optical tables. Peristaltic pumps were used to fill or rinse the compartments of the flow-through cell holding the MIRE. To achieve a relevant signal-to-noise ratio 3000 to 4000 scans (45–60 min measurement time) were necessary for each polarization direction (parallel and perpendicular polarized incident light) in the protein experiments to properly evaluate the surface concentrations. For determining the surface concentration of the silane layers 500 to 1000 scans were sufficient.

### SBSR-measuring technique

As the quantitative IR-spectroscopic detection of molecular monolayers requires extremely accurate and sensitive methods, the single-beam sample-reference (SBSR) measurement method<sup>35</sup> was used to compensate absorbances from bulk water in sample and reference. Fluctuations of the absorbance of remaining water vapor and carbon dioxide during the measurement of sample and reference are also reduced to a minimum by this method. The flow-through cell separates the MIRE horizontally in a sample and a reference compartment. It is attached onto a stage and can be vertically moved in the IR-beam by a computer controlled lift to alternately measure spectra of the sample and reference compartments and allows an outstanding compensation of water absorbance. This is crucial, since proteins are typically quantified according to their amide I (1640  $\text{cm}^{-1}$ ) and amide II (1540  $\text{cm}^{-1}$ ) vibrations, any additional uncompensated water absorbance between sample and reference deteriorates the results. Differences in the transmission properties of the MIRE in the sample and reference compartments were recorded before surface modifications and considered when calculating the final difference spectra of the samples.

### Calculation of the surface concentration

The surface concentration  $\Gamma$  may be understood as the projection of the molecules in the volume defined by unit area and height  $d$  (real sample thickness). As a consequence, surface concentration of a thin layer can be determined without knowing the real thickness  $d$  and its real structure. The calculation is based on Lambert-Beer's law. For the ATR technique the introduction of the so-called "effective thickness"  $d_e$  first introduced by Harrick is required.<sup>20,35,46</sup> The volume concentration  $c$  and the surface concentration  $\Gamma$  are related to each other *via* the thickness  $d$  of the sample. By introducing Lambert-Beer's law one obtains

$$c = \frac{I}{d} = \frac{\int A_{\text{pp|vp}}(\tilde{\nu}) d\tilde{\nu}}{Nnd_{\text{e,pp|vp}}^{\text{th}} \int \epsilon(\tilde{\nu}) d\tilde{\nu}} \quad (1)$$

$\int A_{\text{pp|vp}}(\tilde{\nu}) d\tilde{\nu}$  denotes the integrated absorbance of a distinct absorbance band measured with parallel (pp), or perpendicular (vp) polarized incident light, respectively.  $N$  is the mean number of the active internal reflections and  $n$  denotes the number of equal infrared active groups per molecule leading to the absorbance of the evaluated bands.  $\int \epsilon(\tilde{\nu}) d\tilde{\nu}$  denotes the common integrated molar absorption coefficient of the vibrational mode of one infrared active group.  $d_{\text{e,pp|vp}}^{\text{th}}$  is the effective thickness of the layer which depends on the polarization, the angle of incidence and the refractive indices of the MIRE and the sample.  $d_{\text{e,pp|vp}}^{\text{th}}$  is regarding the theory of ATR the crucial value to be determined. In the case of anisotropic samples (1) would lead to different results for parallel and vertical polarized light. Therefore the absorbance of both polarization directions has to be determined and to be considered in the calculation of the surface concentration using a model for the orientation of the molecules.<sup>35</sup> Here we used the model of liquid crystalline ultrastructure (LCU) for the calculation of surface concentrations. This model best fits the distribution of orientation of silanes and is also correct for isotropic distributions of molecules. For proteins the isotropic distribution was ensured by the determination of the dichroic ratio  $R_{\text{exp}}$ . Eqn (2) that has to be equal to the theoretical dichroic ratio  $R_{\text{iso}}^{\text{th}} = 1.63$  that is valid for thin layers and the used optical parameters of ATR measurements.

$$R_{\text{exp}} = \frac{\int A_{\text{pp}}(\tilde{\nu}) d\tilde{\nu}}{\int A_{\text{vp}}(\tilde{\nu}) d\tilde{\nu}} \quad (2)$$

As in the experiments with TNF- $\alpha$  the signal-to-noise ratio of the vp-measurements was very poor, the surface concentrations of TNF- $\alpha$  and its antibody were directly determined by the evaluation of eqn (1) using results from pp measurements. The reader is referred to ref. 20,34,35 and 46 for more details of the quantitative evaluation of molecular surface densities using the ATR technique. Optical parameters used in the calculations are  $45^\circ \pm 5^\circ$  angle of incidence, and refractive indices at wavenumber  $1540 \text{ cm}^{-1}$  for silicon ( $3.42 \pm 0$ ), water ( $1.33 \pm 0.06$ ) and sample layer ( $1.45 \pm 0.06$ ). The number of active internal reflections was different in different experiments and is given in Fig. 2. Quantifications for all proteins were done by determining the absorbance of the amide II band that is only barely affected by uncompensated water absorbance. Nevertheless, the integrated absorbance was evaluated after compensation of the small negative water band at  $1640 \text{ cm}^{-1}$  by adding an appropriate amount of a pure water spectrum. We emphasize that this small amount of uncompensated water results from water present in the reference compartment but replaced by the molecules of the bound layer in the sample compartment and therefore it can never be experimentally removed. The amount of added water absorbance was estimated by the remaining absorbance of the  $\text{H}_2\text{O}$  stretching vibration and by evaluating the ratio between

integrated absorbances of amide I and amide II vibrations. The resulting ratios were between 1.45 and 2.68 with a mean value of 2.25 for parallel polarized light and between 2.21 and 3.81 with a mean value of 2.63 for vertical polarized light. Estimated values of the error of integrated absorbances are between 5% and 30% depending on the signal-to-noise levels of spectra and remaining uncompensated water absorption. All errors in the calculation of surface concentrations and dichroic ratios are evaluated using propagation of uncertainty.

### Determination of molar absorption coefficients

FTIR transmission-spectra of 3-(trimethoxy) butylsilyl aldehyde dissolved in different concentrations in 96% EtOH were measured and integrated absorbances of the C=O vibration were determined using integration limits of  $1751 \pm 1$  and  $1693 \pm 1 \text{ cm}^{-1}$  (peak maximum at  $1717 \text{ cm}^{-1}$ ). The resulting average integral molar absorption coefficient of the C=O vibration of 3-(trimethoxy) butylsilyl aldehyde was  $8.6 \times 10^5 (\pm 2.9 \times 10^5) \text{ cm mol}^{-1}$ . Ethanolamine was dissolved in 10 mM phosphate buffer and the integrated absorbance of the  $\text{CH}_2$  symmetric stretch vibration was determined. The integration limits were set at  $2867 \pm 1$  and  $2831 \pm 1 \text{ cm}^{-1}$  (peak maximum at  $2853 \text{ cm}^{-1}$ ). The resulting molar absorption coefficient was  $1.18 \times 10^6 \text{ cm mol}^{-1}$ . The value for the molar absorption coefficient of one amide bond of the amide II vibrational mode of BSA was determined by Reiter *et al.*<sup>19</sup> as  $8.25 \times 10^6 \text{ cm mol}^{-1}$  with integration limits at  $1585 \pm 1$  and  $1500 \pm 1 \text{ cm}^{-1}$  (for proteins, the molar absorption coefficient is related to single amide bondings and not to the whole molecule).

### Silanization of silicon MIREs using 3-(trimethoxy)butylsilyl aldehyde

According to the protocol of Patolsky *et al.*<sup>14</sup> a solution of 1% 3-(trimethoxy)butylsilyl aldehyde in 96% EtOH was filtered with a  $20 \mu\text{m}$  cut-off PTFE syringe filter after a 20 min waiting period and pumped into the sample compartment of the flow-through cell. The reaction time to form hydrogen bonds with the silanol groups (Fig. 1) of the silicon-oxide surface was 30 min. Afterwards, the sample-compartment was carefully rinsed with 96% ethanol ( $2 \mu\text{l s}^{-1}$ ) to flush out any unbound silane. After drying with nitrogen gas, the system was exposed to a temperature of  $80^\circ \text{C}$  for 30 min to form covalent bonds between silane and the silicon-oxide surface. Precursor experiments showed that these parameters lead to a high surface concentration of covalently bound silane. As last step, the silane layer on silicon is thoroughly rinsed with 96% EtOH to remove any non-covalently bound silane from the surface with a flow rate of  $15 \mu\text{l s}^{-1}$ . The silane surface concentration of every silanization was quantified to ensure consistent and uniform conditions for subsequent protein attachment.

### Protein binding to aldehyde surface

The proteins are either reconstituted or diluted in 10 mM sodium or potassium phosphate buffer with a pH of 8.4 additionally containing 4 mM sodium cyanoborohydride ( $\text{NaBH}_3\text{CN}$ ). The protein solution was pumped over the silanised surface through the sample-compartment of the flow-through cell with a very low

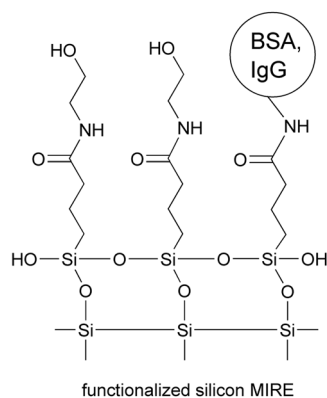
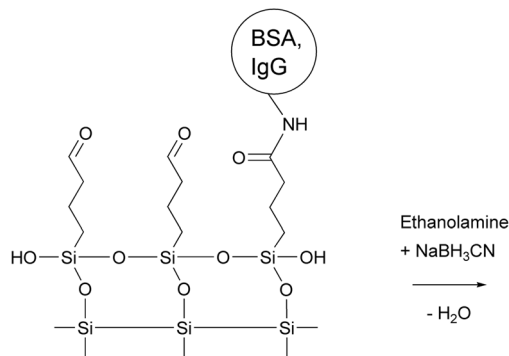
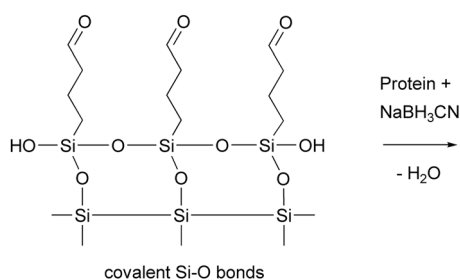
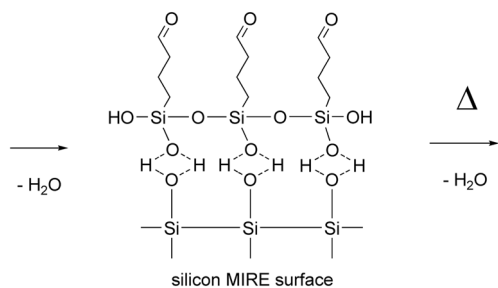
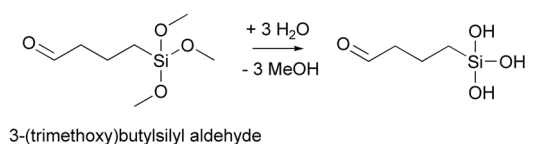


**Fig. 1** Chemical scheme of surface functionalization of a silicon MIRE with 3-(trimethoxy)butylsilyl aldehyde and covalent bonding of proteins.

flow rate of  $42 \mu\text{l min}^{-1}$  avoiding any depletion effects. Free amino groups of the proteins can then form imines (Schiff's bases) with the aldehyde moieties of the silane layer.

Subsequently imines are reduced by cyanoborohydride to amide bonds leading to covalent bonding of proteins and silane. After a 2 h reaction period, superfluous protein was washed out by rinsing with buffer solution.

### Passivation of aldehyde surface

Since not every aldehyde moiety of the silane layer binds proteins, the remaining CHO groups must be capped to prevent any unspecific binding in further antibody experiments. This was done by filling the sample-compartment for 2 h with 100 mM ethanolamine containing 4 mM cyanoborohydride in a phosphate buffer at a pH of 8.4.

### Antigen capturing with antibody layer

Antigen solutions of TNF- $\alpha$  and PSA in phosphate buffer with a pH of 7.4 were pumped onto the respective antibody layers and left for 2 h to ensure thorough antigen-antibody contact. Afterwards superfluous antigen that was not bound to the antibodies was washed out with phosphate buffer.

## Results and discussion

### Surface concentration of 3-(trimethoxy)butylsilyl aldehyde

3-(Trimethoxy)butylsilyl aldehyde was covalently bound to the silicon-oxide surface serving as a basic linker molecule for all further chemical modification steps. The measured surface concentrations evaluated from the absorbance of the C=O vibration (Fig. 2A) were between  $6.0 \times 10^{-10} \text{ mol cm}^{-2}$  and  $1.2 \times 10^{-9} \text{ mol cm}^{-2}$  with optimized protocols for silanization. A theoretical value of the surface concentration of a densely packed monolayer can be estimated by simple two-dimensional geometrical calculations of the molecule<sup>47</sup> and results in  $4.88 \times 10^{-10} \text{ mol cm}^{-2}$ , which perfectly matches our measured values. Differences in surface concentrations can be caused by the nanoscale surface roughness of the MIRE resulting in an increased surface area and by the polymerization processes of trimethoxy silanes that can lead to different chain lengths and therefore a multilayer arrangement.<sup>48</sup> Indeed, already small changes in the preparation protocols such as the curing temperature and time, treatment of the semiconductor surface or the dwell-time of silane before the start of polymerization led to highly differing surface concentrations up to  $2.0 \times 10^8 \text{ mol cm}^{-2}$  in preliminary experiments. Only by the use of the quantitative evaluation of this step, we were able to establish a preparation protocol leading to reproducible and meaningful results.

### Bovine serum albumin (BSA) on aldehyde silane layer

Since BSA is one of the most used and best characterized proteins, a measurement system was developed to determine the surface concentration and the workability of the linker protocol. BSA is known to exhibit considerable adhesion and to form densely packed layers on a variety of surfaces including germanium MIREs in IR-spectroscopy,<sup>49–51</sup> mica platelets<sup>52</sup> and gold stripes<sup>53</sup> used in atomic force microscopy. The number of functional amide bonds is 582. Following experiments were conducted to determine the maximum possible surface concentration

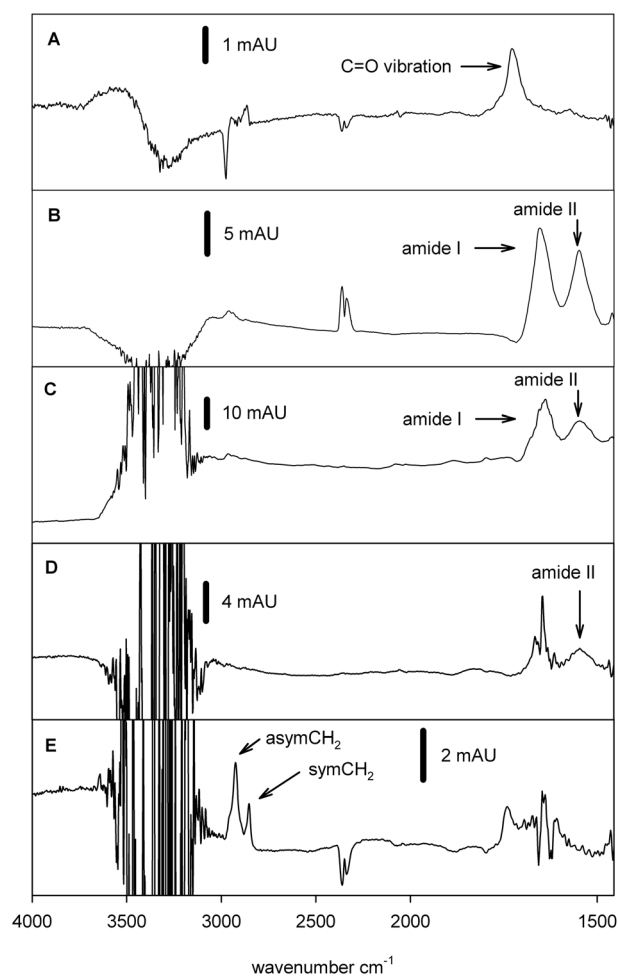


**Fig. 2** FTIR-ATR absorbance spectra of single components for the setup of an antibody/antigen biosensor. Spectra were measured *in situ* during the layer by layer formation. (A) FTIR-ATR absorbance spectrum of 3-(trimethoxy)butylsilyl aldehyde in 96% ethanol. The quantitatively evaluated band is the C=O (carbonyl) vibration of the tail-group of the used silane (see Fig. 1 for structure) at  $1720\text{ cm}^{-1}$ . It indicates free carbonyl groups of silane on the silicon-oxide surface ready to form imine bonds. Other bands are caused by EtOH and H<sub>2</sub>O incompenations despite the SBSR measurement method. Reference was blank silicon. Spectrum recorded with 1000 scans. (B) FTIR-ATR absorbance spectrum of BSA on aldehyde silane surface. The amide I ( $1640\text{ cm}^{-1}$ ) and amide II ( $1540\text{ cm}^{-1}$ ) bands are clearly distinguishable. Only the amide II band is used for the quantitative evaluation of the surface concentration, because amide I can be overlapped by uncompensated absorption of the water bending vibration. Other prominent bands are incompenations of the H<sub>2</sub>O stretching vibration at  $3400\text{ cm}^{-1}$  and the gaseous CO<sub>2</sub> stretching vibration at  $2400\text{ cm}^{-1}$ . Reference was silanised silicon. Spectrum recorded with 3000 scans. (C) FTIR-ATR absorbance spectrum of anti-PSA antibody on aldehyde silane surface. Reference was silanised silicon. Recorded with 3000 scans. (D) FTIR-ATR absorbance spectrum of prostate specific antigen (PSA) on antibody surface. Reference was the ethanolamine passivated antibody layer on silanised silicon. Spectrum recorded with 3000 scans. (E) FTIR-ATR absorbance spectrum of ethanolamine on antibody surface. The symmetric CH<sub>2</sub> vibration was quantified. Reference was the antibody layer on silanised silicon. Spectrum recorded with 3000 scans. Spectroscopic parameters for all experiments were silicon MIRE,  $45^\circ$  angle of incidence and 10 mM phosphate buffer. Number of active internal reflections:  $26(\pm 1)$  for TNF- $\alpha$ ,  $28(\pm 1)$  for PSA experiments.

of BSA covalently bound on an aldehyde-silanised silicon-oxide surface. We utilized a solution of BSA with a concentration of  $100\text{ }\mu\text{g ml}^{-1}$  prepared in 10 mM phosphate buffer at a pH of 7.4 and pumped it into the flow-through cell containing the silanised surface of a silicon MIRE. The protein solution was allowed to adsorb for 2 h followed by a buffer rinse to remove the bulk protein solution. Adsorption of BSA was investigated by evaluating the absorbance of the amide II vibration (Fig. 2B). Resulting BSA surface concentrations were in the range of  $5.62\text{--}7.17 \times 10^{-13}\text{ mol cm}^{-2}$ . This means one molecule of BSA is found within an area of  $295\text{ nm}^2$  to  $232\text{ nm}^2$ . Compared to the maximum achievable surface concentration of  $5.7 \times 10^{-12}\text{ mol cm}^{-2}$  documented by Hassler<sup>54</sup> the values are lower by an order of magnitude. However the experimental conditions were significantly different. Hassler used a germanium MIRE, a  $25\text{ mg ml}^{-1}$  protein concentration and high concentrations of sodium chloride, which shields the charges of the proteins<sup>39,55</sup> and the germanium surface, ultimately forming a BSA monolayer. Albumins mainly act as transport molecules in a living body and are known to be capable of binding chloride ions.<sup>56</sup> Luey *et al.*<sup>57</sup> showed that an increase in ionic strength leads to higher surface concentrations on silicon due to the shielding effect negatively charged ions have on the protein itself. Although in our experimental setup the surface charges of the silanol groups are blocked by the aldehyde silane, electrostatic repulsion between the individual BSA molecules is still taking place possibly leading to a reduced surface concentration.

#### Surface concentrations of anti-TNF- $\alpha$ antibody on silanised silicon and captured TNF- $\alpha$

The antibody/antigen system anti-TNF- $\alpha$  antibody and TNF- $\alpha$  was investigated using the bound antibody as receptor molecules to specifically bind its antigen that should be detected in the case of a biosensor. The number of functional amide bonds of all IgG antibodies is  $1320 (\pm 4)$  and the number of functional amide bonds of TNF- $\alpha$  is 468. A protein solution of  $100\text{ }\mu\text{g ml}^{-1}$  of anti-TNF- $\alpha$  antibody in 10 mM sodium phosphate buffer at pH 8.4 was pumped onto an aldehyde silane layer with additional 4 mM cyanoborohydride. After 2 hours, the bulk protein solution including only adhered antibody was flushed out with buffer solution at pH 7.4. Quantification of the amide II vibrations in this state resulted in surface concentrations between  $1.6 \times 10^{-13}\text{ mol cm}^{-2}$  and  $1.7 \times 10^{-13}\text{ mol cm}^{-2}$  for the anti-TNF- $\alpha$  antibody. This corresponds to a used area of  $1000\text{ nm}^2$  per molecule or a side length of 31 nm assuming square cross-sections. The diameter of IgG antibodies differs in the literature between 16 nm (ref. 58) and 28 nm,<sup>59</sup> corresponding to required area per molecule of  $256\text{ nm}^2$  to  $784\text{ nm}^2$  assuming square cross-sections. Therefore, in the case of anti-TNF- $\alpha$  antibody an almost closed monolayer bound to the silanised surface can be supposed. After providing TNF- $\alpha$  bulk concentrations between  $1\text{ }\mu\text{g ml}^{-1}$  and  $18\text{ }\mu\text{g ml}^{-1}$  to the bound anti-TNF- $\alpha$  antibody molecules, the surface concentration of antibody-bound TNF- $\alpha$  resulted in  $1.7 \times 10^{-13}\text{ mol cm}^{-2}$  to  $2.7 \times 10^{-13}\text{ mol cm}^{-2}$  corresponding to an antigen/antibody ratio between 1.0 and 1.6 (Fig. 3). Since one IgG antibody molecule can at best bind two antigens, this shows that almost all possible binding sites of the antibody specifically bound antigens. Below a bulk concentration of  $1\text{ }\mu\text{g ml}^{-1}$ , TNF- $\alpha$

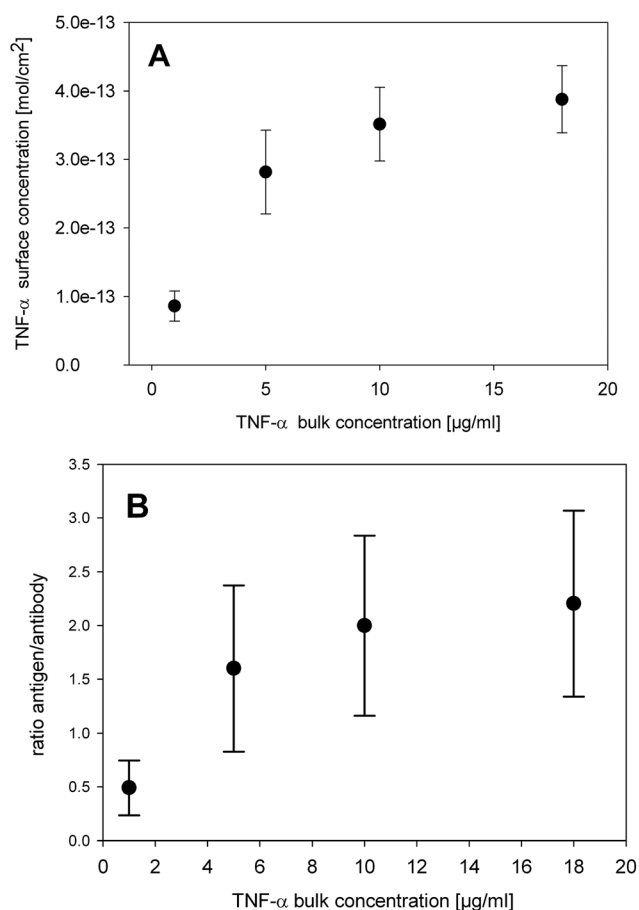


**Fig. 3** (A) TNF- $\alpha$  surface concentrations resulting from specific binding to anti-TNF- $\alpha$  antibody with a surface concentration of  $1.76 \times 10^{-13}$  mol cm<sup>-2</sup>. (B) The ratio of antigen to antibody exhibits the expected exponential shape asymptotically approaching the value of two, which is the maximum possible binding capability of an IgG antibody.

could neither be detected in the bulk solution nor captured on the surface. The smallest detectable absorption amplitude in the amide II region was 50  $\mu$ AU for parallel polarized light. This corresponds to a peak integral of about  $2.7 \times 10^{-3}$  cm<sup>-1</sup> resulting in a detection limit for TNF- $\alpha$  of  $2.6 \times 10^{-14}$  mol cm<sup>-2</sup>.

#### Anti-PSA-antibody and PSA on the aldehyde surface

As a second antibody/antigen system PSA-antibody and PSA was investigated. This system was already used in a prototype nanosensor by Patolsky *et al.*<sup>14</sup> Here the number of amide bonds of PSA is 237. A solution of mouse anti-PSA antibody with a concentration of 50  $\mu$ g ml<sup>-1</sup> in 10 mM potassium phosphate buffer at a pH of 8.4 and additional 4 mM cyanoborohydride was pumped onto the aldehyde surface and left for 2 h (Fig. 2C). Surface concentrations of PSA-antibody were determined in the range of  $3.2$ – $6.1 \times 10^{-13}$  mol cm<sup>-2</sup>. The area used by each antibody molecule was in the range of 270 nm<sup>2</sup> to 520 nm<sup>2</sup>. Again, this agrees very well with the required area per molecule for an IgG antibody. After passivation with ethanolamine various PSA-antigen concentrations in the range of 5 ng ml<sup>-1</sup> to 10  $\mu$ g ml<sup>-1</sup> in 10 mM potassium phosphate buffer, pH 7.4 with additional 2  $\mu$ M KCl were slowly pumped (42  $\mu$ l min<sup>-1</sup>) over the antibody

surface for 2 h (Fig. 2D). The calculated antigen surface concentrations could be determined to be between  $1.6 \times 10^{-13}$  mol cm<sup>-2</sup> and  $7.0 \times 10^{-13}$  mol cm<sup>-2</sup>. The resulting ratio of antigen to antibody could be determined between 0.3 and 1.4, again showing a suitable value for specific binding of the antigen (Fig. 4). In PSA-antigen solutions with concentrations between 5 ng ml<sup>-1</sup> and 500 ng ml<sup>-1</sup> evaluable amide vibration bands of the antigen could be detected neither in the spectra of the bulk solution nor in the spectra of the layer after washing. The smallest detectable amplitude for PSA was 100  $\mu$ AU for parallel polarized light. This corresponds to a peak integral of about  $5 \times 10^{-3}$  cm<sup>-1</sup> resulting in a detection limit of the surface concentration of  $5.13 \times 10^{-14}$  mol cm<sup>-2</sup>. To determine the concentration of ethanolamine used for surface passivation after protein binding, we evaluated the increase of absorbance of the symmetric CH<sub>2</sub> vibration resulting from the passivation step (Fig. 2E). The ethanolamine surface concentration was  $2.30 \times 10^{-10}$  mol cm<sup>-2</sup> in PSA experiments. This means that about one-third of the aldehyde moieties of the silane layer are capped with ethanolamine after PSA was bound to the silane.

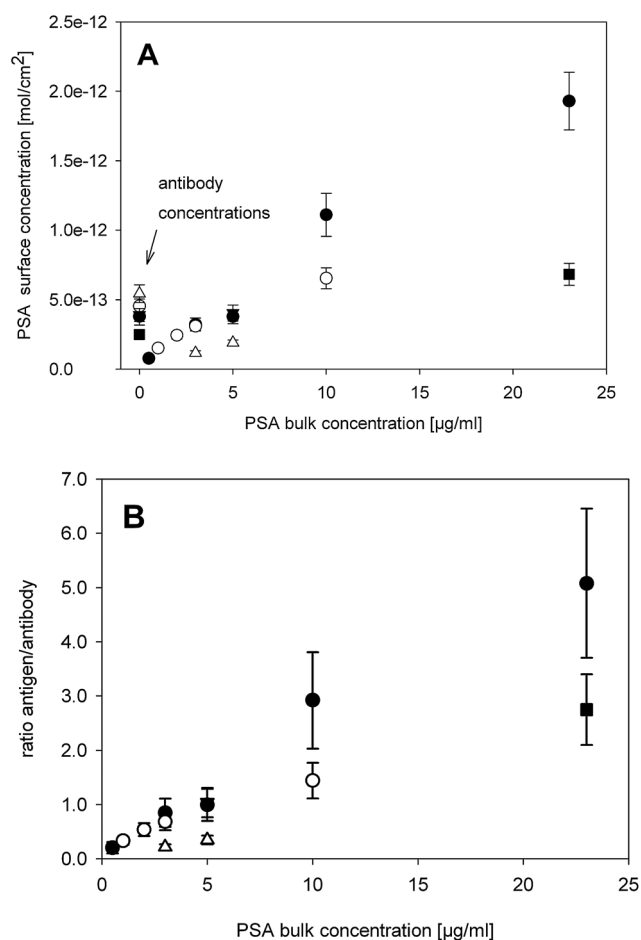


**Fig. 4** (A) PSA surface concentrations on anti-PSA antibody surface in five different experiments. Antibody concentration of each experiment is shown at a bulk concentration of zero. (B) Ratio of antigen to antibody in several experiments. Since two antigens is the maximum possible binding capability of an IgG antibody values exceeding two points to unspecific adhesion to the surface. This occurred only in one experiment at very high bulk concentrations of the antibody.

**Table 1** Surface concentrations of single molecule layers

Molecule	Concentration of bulk solution	Measured surface concentration/ mol cm <sup>-2</sup>	Error of surface concentration/ mol cm <sup>-2</sup>	Corresponding area per molecule/nm <sup>2</sup>	Required area per molecule in literature/ nm <sup>2</sup>	Molecular weight/ g mol <sup>-1</sup>	Surface mass concentration/ ng cm <sup>-2</sup>	Error of surface mass conc./ ng cm <sup>-2</sup>
3-(Trimethoxy)butylsilyl aldehyde	10 mg ml <sup>-1</sup>	7.0 × 10 <sup>-10</sup>	1.10 × 10 <sup>-10</sup>	0.23	0.34	192.3	135	21.3
BSA	100 µg ml <sup>-1</sup>	5.62 × 10 <sup>-13</sup> to 7.17 × 10 <sup>-13</sup>	9.79 × 10 <sup>-14</sup> to 1.17 × 10 <sup>-13</sup>	295–232	56 (ref. 19)	66 440	37.3–47.6	6.5–7.7
Anti-TNF-α	100 µg ml <sup>-1</sup>	1.6 × 10 <sup>-13</sup> to 1.7 × 10 <sup>-13</sup>	4.68 × 10 <sup>-14</sup>	1100–970	784, (ref. 59) 256–361 (ref. 58)	146 000	23.4–24.8	6.8
Anti-PSA	50 µg ml <sup>-1</sup>	3.2 × 10 <sup>-13</sup> to 6.1 × 10 <sup>-13</sup>	3.0 × 10 <sup>-14</sup> to 6.0 × 10 <sup>-14</sup>	520–270	784, (ref. 59) 256–361 (ref. 58)	~150 000	48.0–91.5	4.5–9.0
TNF-α	1–18 µg ml <sup>-1</sup>	8.61 × 10 <sup>-14</sup> to 3.88 × 10 <sup>-13</sup>	2.2 × 10 <sup>-14</sup> to 4.12 × 10 <sup>-14</sup>	Ratio: TNF-α/anti-TNF-α, 0.5–2.2		52 100	4.5–20.2	1.2–2.2
PSA	0.5–10 µg ml <sup>-1</sup>	7.7 × 10 <sup>-14</sup> to 7.0 × 10 <sup>-13</sup>	1.68 × 10 <sup>-14</sup> to 7.9 × 10 <sup>-14</sup>	Ratio: PSA/anti-PSA, 0.2–3 (5.1)		34 000	2.6–23.8	0.57–2.7

## Conclusions

Regarding the use of semiconductors as transducers, we point out that the resulting surface concentration of bound molecules on such surfaces is very sensitive to a variety of parameters of the surface chemistry used. With the ability of quantitative analysis of each layer, one can detect unexpected results in an early stage of the surface modification. We showed that it is possible to cover the whole silanised surface with an almost compact monolayer only showing a slightly different surface concentration for different proteins (Table 1). As the proteins used are of the same size, the differences likely result from the different partial charges of the proteins. Thus it is possible to cover semiconductor nanostructures with a compact monolayer of receptor molecules for sensing purposes. Again, we want to emphasize that the optimum result of a compact monolayer is easily disrupted by non-optimal steps in the surface modification. It is a time consuming procedure to find the reasons for varying results without the ability to quantitatively assess each step during surface functionalization.

Antigen–antibody binding can be well detected and quantified by the present method when the bulk concentration of the antigen is above 1 µg ml<sup>-1</sup>. This shows that almost all possible binding sites of the antibody are able to bind antigens. Therefore achievable surface concentrations of target molecules are only limited by the size of the receptor molecules and their binding sites, unless the molecules are highly charged.

ATR-FTIR spectroscopy was shown to detect molecular surface concentrations of proteins in aqueous environment down to the 20 fmol cm<sup>-2</sup> range. This is only about one order of magnitude higher than reported for the most sensitive surface plasmon field-enhanced fluorescence spectroscopy,<sup>60</sup> where surface concentrations of DNA strands were measured down to 1 fmol cm<sup>-2</sup>.<sup>61</sup> Despite the smaller sensitivity, ATR-FTIR spectroscopy has considerable advantages in label-free detection and provides direct chemical information on detected molecules.

The detection of such small infrared absorptions in aqueous solutions can only be achieved using multiple reflection ATR

elements combined with a high number of scans that result in long measurement times (up to two hours for one layer). Enhanced methods such as the SBSR technique used here are probably necessary to compensate long-term drifts between sample and reference. Further enhanced methods like modulated excitation could improve the detection limit by at least one order of magnitude when the detectable molecules can be reversibly excited, e.g. by pH or temperature modulation.<sup>23,34</sup>

## Acknowledgements

We thank Prof. Wolfgang Lindner of the Chemical Faculty of the University of Vienna for his assistance in silane chemistry and the facilitation of the silanization protocol and Prof. Falkenhagen of the Danube University, Krems (Austria) for providing us with monoclonal hTNF-α antibody. This work has been financially supported by Austrian Science Fund (FWF) Project No. P20871-N31 and by Award No. KUK-I1-007-43, made by the King Abdullah University of Science and Technology (KAUST). We dedicate this article to the memory of Prof. Urs Peter Fringeli.

## References

- H. Hunt and A. Armani, *Nanoscale*, 2010, **2**, 1544–1559.
- E. Stern, J. F. Klemic, D. A. Routenberg, P. N. Wyrembak, D. B. Turner-Evans, A. D. Hamilton, D. A. LaVan, T. M. Fahmy and M. A. Reed, *Nature*, 2007, **445**, 519–522.
- N. Backmann, C. Zahnd, F. Huber, A. Bietsch, A. Plückthun, H.-P. Lang, H.-J. Güntherodt, M. Hegner and C. Gerber, *Proc. Natl. Acad. Sci. U. S. A.*, 2005, **102**, 14587–14592.
- E. Stern, A. Vacic, N. K. Rajan, J. M. Criscione, J. Park, B. R. Ilic, D. J. Mooney, M. A. Reed and T. M. Fahmy, *Nat. Nanotechnol.*, 2010, **5**, 138–142.
- E. Benesa, M. Gröschla, W. Burgera and M. Schmid, *Sens. Actuators, A*, 1995, **48**, 1–21.
- L. Pang, J. Li, J. Jiang, G. Shen and R. Yu, *Anal. Biochem.*, 2006, **358**, 99–103.
- X. Wang, J. Zhou, J. Song, J. Liu, N. Xu and Z. L. Wang, *Nano Lett.*, 2006, **6**, 2768–2772.
- L. G. Carrascosa, M. Moreno, M. Alvarez and L. M. Lechuga, *TrAC, Trends Anal. Chem.*, 2005, **25**, 196–206.

- 9 L. M. Lechuga, J. Tamayo, M. Álvarez, L. G. Carrascosa, A. Yufera, R. Doldán, E. Peralías, A. Rueda, J. A. Plaza, K. Zinoviev, C. Domínguez, A. Zaballos, M. Moreno, C. Martínez-A, D. Wenn, N. Harris, C. Bringer, V. Bardinal, T. Camps, C. Vergnenègre, C. Fontaine, V. Diaz and A. Bernad, *Sens. Actuators, B*, 2006, **118**, 2–10.
- 10 P. Dutta, K. Hill, P. G. Datskos and M. J. Sepaniak, *Lab Chip*, 2007, **7**, 1184–1191.
- 11 J. H. Lee, K. S. Hwang, J. Park, K. H. Yoon, D. S. Yoon and T. S. Kim, *Biosens. Bioelectron.*, 2005, **20**, 2157–2162.
- 12 J. I. Hahm and C. M. Lieber, *Nano Lett.*, 2004, **4**, 41–54.
- 13 D. S. Kim, J. E. Park, J. K. Shin, P. K. Kim, G. Lim and S. Shoji, *Sens. Actuators, B*, 2006, **117**, 488–494.
- 14 F. Patolsky, G. Zheng and C. M. Lieber, *Nat. Protoc.*, 2006, **1**, 1711–1724.
- 15 J. A. Ferguson, F. J. Steemers and D. R. Walt, *Anal. Chem.*, 2000, **72**, 5618–5624.
- 16 G. Zheng, F. Patolsky, Y. Cui, W. U. Wang and C. M. Lieber, *Nat. Biotechnol.*, 2005, **23**, 1294–1301.
- 17 C. Y. Hsiao, C. H. Lin, C. H. Hung, C. J. Su, Y. R. Lo, C. C. Lee, H. C. Lin, F. H. Ko, T. Y. Huang and Y. S. Yang, *Biosens. Bioelectron.*, 2009, **24**, 1223–1229.
- 18 J. Kim, J. Cho, P. M. Seidler, N. E. Kurland and V. K. Yadavalli, *Langmuir*, 2010, **26**, 2599–2608.
- 19 G. Reiter, N. Hassler, V. Weber, D. Falkenhagen and U. P. Fringeli, *Biochim. Biophys. Acta*, 2004, **1699**, 253–261.
- 20 N. Hassler, D. Baurecht, G. Reiter and U. P. Fringeli, *J. Phys. Chem. C*, 2011, **115**, 1064–1072.
- 21 C. Nowak, M. G. Santonicola, D. Schach, J. Zhu, R. B. Gennis, S. Ferguson-Miller, D. Baurecht, D. Walz, W. Knoll and R. L. C. Naumann, *Soft Matter*, 2010, **6**, 5523–5532.
- 22 J. Matijasevic, N. Hassler, G. Reiter and U. P. Fringeli, *Langmuir*, 2008, **24**, 2588–2596.
- 23 D. Baurecht, G. Reiter, N. Hassler, M. Schwarzott and U. P. Fringeli, *Chimia*, 2005, **59**, 226–235.
- 24 J. M. Andanson and A. Baiker, *Chem. Soc. Rev.*, 2010, **39**, 4571–4584.
- 25 S. Reimann, A. Urakawa and A. Baiker, *J. Phys. Chem. C*, 2010, **114**, 17836–17844.
- 26 M. Mueller and B. Kessler, *Langmuir*, 2011, **27**, 12499–12505.
- 27 M. Mueller, W. Ouyang and B. Kessler, *Spectrochim. Acta, Part A*, 2010, **77**, 709–716.
- 28 A. M. Popa, S. Angeloni, T. Buergi, J. A. Hubbell, H. Heinzelmann and R. Pugin, *Langmuir*, 2010, **26**, 15356–15365.
- 29 B. Panella, A. Vargas, D. Ferri and A. Baiker, *Chem. Mater.*, 2009, **21**, 4316–4322.
- 30 D. M. Meier, A. Urakawa, R. Mäder and A. Baiker, *Rev. Sci. Instrum.*, 2008, **80**, 094101–094111.
- 31 A. Vargas, I. Shnitko, A. Teleki, S. Weyeneth, S. E. Pratsinis and A. Baiker, *Appl. Surf. Sci.*, 2010, **257**, 2861–2869.
- 32 O. Taratula, E. Galoppini and R. Mendelsohn, *Langmuir*, 2009, **25**, 2107–2113.
- 33 R. Mendelsohn, G. Mao and C. R. Flach, *Biochim. Biophys. Acta, Biomembr.*, 2010, **1798**, 788–800.
- 34 U. P. Fringeli, in *Internal Reflection Spectroscopy*, ed. F. M. Mirabella, Jr, CRC Press, New York, 1992, pp. 255–324.
- 35 U. P. Fringeli, D. Baurecht, T. Bürgi, M. Siam, G. Reiter, M. Schwarzott and P. Brüesch, in *Handbook of Thin Film Materials*, ed. H. S. Nalwa, Academic Press, San Diego (USA), 2002, vol. 2, pp. 191–229.
- 36 C. Heitzinger, Y. Liu, N. Mauser, C. Ringhofer and R. W. Dutton, *J. Comput. Theor. Nanosci.*, 2010, **7**, 2574–2580.
- 37 C. Heitzinger, N. Mauser and C. Ringhofer, *SIAM J. Appl. Math.*, 2010, **70**, 1634–1654.
- 38 S. Baumgartner and C. Heitzinger, *Commun. Math. Sci.*, 2012, **10**, 693–716.
- 39 A. Bulyha and C. Heitzinger, *Nanoscale*, 2011, **3**, 1608–1617.
- 40 L. De Vico, L. Iversen, M. H. Sørensen, M. Brandbyge, J. Nygård, K. L. Martinez and J. H. Jensen, *Nanoscale*, 2011, **3**, 3635–3640.
- 41 L. De Vico, M. H. Sørensen, L. Iversen, D. M. Rogers, B. S. Sørensen, M. Brandbyge, J. Nygård, K. L. Martinez and J. H. Jensen, *Nanoscale*, 2011, **3**, 706–717.
- 42 S. Baumgartner, M. Vasicek and C. Heitzinger, *Analysis of Field-Effect Biosensors Using Self-consistent 3D Drift-Diffusion and Monte-Carlo Simulations*, Proc. EuroSensors XXV, Athens, September 2011.
- 43 S. Baumgartner, M. Vasicek, A. Bulyha and C. Heitzinger, *Nanotechnology*, 2011, **22**(425503), 1–8.
- 44 S. Baumgartner, M. Vasicek and C. Heitzinger, *Procedia Eng.*, 2011, **25**, 407–410.
- 45 H. Guenzler and H. U. Gremlich, *IR-Spektroskopie*, Wiley-VCH, Weinheim, 2000.
- 46 N. J. Harrick, *Internal Reflection Spectroscopy*, Harrick Sci. Corp., Ossining (New York), 1979.
- 47 J. Matijasevic, PhD thesis, University of Vienna, 2008.
- 48 J. Zhang, J. Hoogboom, P. H. J. Kouwer, A. E. Rowan and T. Rasing, *J. Phys. Chem. C*, 2008, **112**, 20105–20108.
- 49 T. Maruyama, S. Katoh, M. Nakajima, H. Nabetani, T. P. Abbott, A. Shono and K. Satoh, *J. Membr. Sci.*, 2001, 192.
- 50 K. Murayama and M. Tomida, *Biochemistry*, 2004, **42**, 11526–11532.
- 51 Y. S. Wei, S. Y. Lin, S. L. Wang, M. J. Li and W. T. Cheng, *Biopolymers*, 2003, **72**, 345–351.
- 52 O. Mori and T. Imae, *Colloids Surf., B*, 1997, **9**, 31–36.
- 53 M. Tencera, R. Charbonneau, N. Lahouda and P. Berini, *Appl. Surf. Sci.*, 2007, **253**, 9209–9214.
- 54 N. Hassler, PhD thesis, University of Vienna, 2008.
- 55 Y. S. Lin and V. Hlady, *Colloids Surf., B*, 1994, **2**, 481–491.
- 56 G. Scatchard and W. T. Yap, *J. Am. Chem. Soc.*, 1964, **86**, 3434.
- 57 J. K. Luey, J. McGuire and R. D. Sproull, *J. Colloid Interface Sci.*, 1991, **143**, 489–500.
- 58 R. L. Brady, R. E. Hubbard, D. J. King, D. C. Low, S. M. Roberts and R. J. Todd, *J. Mol. Biol.*, 1991, **219**, 603.
- 59 C. J. Roberts, P. M. Williams, J. Davies, A. C. Dawkes, J. Sefton, J. C. Edwards, A. G. Haymes, C. Bestwick, M. C. Davies and S. J. B. Tendler, *Langmuir*, 1995, **11**, 1822–1826.
- 60 T. Liebermann and W. Knoll, *Colloids Surf., A*, 2000, **171**, 115–130.
- 61 G. Stengel and W. Knoll, *Nucleic Acids Res.*, 2005, **33**, e69.